# Does the XY Model have an integrable continuum limit?

J. Balog[1], M. Niedermaier[4], F. Niedermayer[2] *,

A. Patrascioiu[3], E. Seiler[4], P. Weisz[4]

[1]*Research Institute for Particle and Nuclear Physics*
*1525 Budapest 114, Hungary*

[2]*Institute for Theoretical Physics, University of Bern*
*CH-3012 Bern, Switzerland*

[3]*Physics Department, University of Arizona*
*Tucson, AZ 85721, U.S.A.*

[4]*Max-Planck-Institut für Physik*
*80805 Munich, Germany*

## Abstract

The quantum field theory describing the massive O(2) nonlinear sigma-model is investigated through two non-perturbative constructions: The form factor bootstrap based on integrability and the lattice formulation as the XY model. The S-matrix, the spin and current two-point functions, as well as the 4-point coupling are computed and critically compared in both constructions. On the bootstrap side a new parafermionic super selection sector is found; in the lattice theory a recent prediction for the (logarithmic) decay of lattice artifacts is probed.

---

*On leave from Eötvös University, Budapest

# 1. Introduction

The XY-model in two dimensions is of prime interest in the field of statistical mechanics, intriguing in particular because of its unusual phase transition. On general grounds one expects that a suitable scaling limit in the high temperature phase gives rise to a massive relativistic quantum field theory (QFT). Though an enormous literature exists on the statistical mechanics aspects of the system, to the best of our knowledge the nature of this QFT has never been systematically explored. As part of a long term project on quantum non-linear sigma models we thus address here the question:

*What are the qualitative and quantitative features of the QFT obtained from the XY-model by taking the massive continuum limit?*

The question is of interest, first in that it highlights the important problem of controlling the approach to the continuum in the lattice formulation of QFTs, and second because the proposed continuum QFT seems to possess a rich, hitherto unknown superselection structure. The problem of controlling the continuum limit of a lattice system based on numerical simulations alone is notoriously difficult for several reasons. (i) First because one often lacks rigorous knowledge of the phase structure and the position(s) of the critical points where the correlation length becomes infinite. (ii) Secondly there are in general no rigorous results on how a quantity approaches its continuum limit as a function of the correlation length, even if the existence of the limit is taken for granted.

Knowledge of (i) and (ii) is crucial not only for quantitative aspects but also for matters of principle, like the status of asymptotic freedom beyond perturbation theory in non-abelian models, or more generally the physical differences or similarities of the continuum limits of (spin) systems with abelian and non-abelian symmetries. So far the application of lattice techniques to the extraction of physical quantities has concentrated on the non-abelian models. This suffers unfortunately from both of the before-mentioned problems (i) and (ii). Concerning (ii), the usual working hypothesis, attributed to Symanzik, is that in (perturbatively) asymptotically free theories, physical quantities approach their continuum limit rather rapidly with power-like corrections $1/\xi^p$, with $p$ a positive integer (up to multiplicative logarithmic corrections).

On the other hand for the XY-model we do have rigorous information on point (i). In particular the model with standard action is known to have two phases, one massless and the other massive [17]. The order of the phase transition has been argued by Kosterlitz and Thouless (KT) [28] to be infinite and this picture has been supported by various numerical studies [19]. Moreover concerning point (ii), one of the present authors (J.B.)

[4], has argued that for a certain class of lattice actions and for certain observables (like the S-matrix or a current two-point function) leading lattice artifacts do not depend on the choice of lattice action and are *calculable*. However, they vanish extremely slowly, generically as inverse powers of the *logarithm* of the correlation length $\xi$ (e.g. $\sim 1/\ln^2 \xi$). One of the goals of the present paper is to test this proposal through extensive numerical simulations. Its derivation takes advantage of the Sine-Gordon description of the KT transition introduced by Amit et. al. [1]. Applying a series of (not entirely rigorous) steps invoking universality and making a sequence of mappings their analysis also entails the tentative identification:

*The massive continuum limit of the XY model is related to the Sine-Gordon (SG) model at its extremal fixed point $\beta_{SG} = \sqrt{8\pi}$, in that both systems share subsets of fields with identical correlation functions.*

Examples of shared fields are the Noether current (proportional to the dual of the gradient of the SG scalar) and the energy momentum tensor. Similar to Coleman's SG–Thirring correspondence [13, 26] the mapping between the fields does not preserve locality in general and is likely not to be strictly one-to-one. Nevertheless the correspondence is very useful because the SG model is integrable and for such systems a direct non-perturbative continuum approach exists to construct the QFT, referred to as the form factor bootstrap. In fact, the SG model is the prototype integrable model and it has played an important role in the development of the form factor bootstrap method. Its bootstrap S-matrix was proposed in [52] and a large part of Smirnov's book [43] is devoted to the study of its soliton form factors, where also the form factors of the SG scalar and the Noether current are given. The second purpose of the present paper is to initiate a *bootstrap construction* of the O(2) model along similar lines. Since the form factor approach is largely blind with respect to the local structure we can borrow many mathematical techniques from the SG model, but the interpretation as form factors of certain local O(2) quantum fields requires careful justification, one strategy being the comparison with lattice simulations. To have a handy terminology we shall refer to the QFT defined through the massive continuum limit of the lattice XY model as the "XY QFT", and to the QFT defined via the form factor bootstrap as the "bootstrap O(2) model". The basic proposition to be tested is that both QFTs coincide.

Generally the problem of operator identification and classification in the bootstrap framework rests on conserved quantum numbers. By definition the O(2) model has a manifest O(2) symmetry. Remarkably on the level of the bootstrap S-matrix and the scattering states a *symmetry enhancement* takes place: They are covariant with respect to a larger

non-abelian quantum group symmetry. It turns out that depending on the nature of certain statistics phases the functional equations characterizing the form factors only have the manifest O(2) symmetry or are covariant with respect to the hidden quantum group symmetry. This implies that the field operators of the bootstrap O(2) QFT fall into two classes: those that are (trivial) O(2) multiplets and those that are members of a nontrivial quantum group multiplet. For example a complete set of scattering states seems to be generated both by the spin field and a *local* parafermion field of Lorentz spin 1/4. Both are relatively nonlocal and the latter is quantum group covariant while the former is not. Also the (one–component) Noether current of the O(2) model is a member of a hidden isospin 1 quantum group triplet, where however the charge $\pm 2$ partners can (already classically) not be expressed as local functions of the spin field. The energy-momentum tensor is a quantum group singlet. In view of the parafermion the O(2) model possesses at least two super selection sectors; the full super selection structure and its relation to the quantum group multiplets remains to be explored.

The lay-out of the paper is as follows. We start by briefly recording the quantities considered and introduce the bootstrap and the lattice formulation. In Section 3 we describe in more detail the bootstrap O(2) model and discuss its quantum group invariance. We proceed with formulating the form factor equations and determine the statistics phases for which they exhibit the enhanced quantum group symmetry. Next the $n \leq 4$ particle candidate form factors of the spin field and the Noether current are obtained. Some details on the quantum group structure and the form factor computation are relegated to appendices.

The subsequent sections all involve lattice simulations, concerning which some general information is first collected in Section 4. Next, we report on measurements of the XY phase shifts using a refinement of the finite size technique first employed by Lüscher and Wolff [31] for the O(3) model. In Section 6 our measurements of the two-point functions of the spin field and the Noether current, and of the renormalized zero momentum coupling $g_R$ are presented. There we also compare the results with those obtained by the form factor computations, improving on our earlier estimate [7]. Finally in Section 7 we attempt some conclusions.

## 2. Bootstrap and Lattice O(2) model

One way to approach the O(2) model is as the $n = 2$ member of the family of $O(n)$ nonlinear $\sigma$-models with the classical Lagrangean

$$\mathcal{L}^{O(n)} = \frac{1}{2g^2} \partial_\mu S^a \partial_\mu S^a , \qquad S^a S^a = 1, \qquad a = 1, 2, \ldots n. \tag{2.1}$$

From the viewpoint of classical field theory it may be surprising that this Lagrangean should correspond to a nontrivial QFT, since by substituting $S_1 = \cos\phi$, $S_2 = \sin\phi$ it becomes quadratic, corresponding to a free theory. Also perturbatively the beta-function of the coupling $g^2$ vanishes identically for $n = 2$, suggesting a trivial scale invariant theory. The situation changes, however, when one is trying to nonperturbatively construct a QFT corresponding to (2.1). In this paper two such approaches are studied, both of which lead to a nontrivial massive QFT: the lattice approach which allows the construction of a massive continuum limit and the form factor bootstrap construction based on the indicated relation to the Sine-Gordon theory. These two constructions as well as the comparison of the resulting theories are the main subject of this investigation.

### 2.1 Quantities to be investigated

Clearly only physical quantities should be considered in this comparison. We shall study the S-matrix, the spin and current two-point functions, and the intrinsic coupling. The S-matrix will be discussed in sections 2.2 and 5; for the other quantities we collect here the key definitions. They apply to both formulations, and in fact to any O(2) invariant scalar relativistic QFT with a mass gap. Let thus $S^a(x)$, $a = 1, 2$, denote a two-component (renormalized) scalar field (the "spin field"). For the Fourier transform of its Euclidean two-point function we write

$$G(k)\delta^{a_1 a_2} = \int d^2 x \, e^{ikx} \langle S^{a_1}(x) S^{a_2}(0) \rangle . \tag{2.2}$$

Its inverse is supposed to have the usual small momentum expansion

$$G(k)^{-1} = Z_{\mathrm{R}}^{-1} \left( M_{\mathrm{R}}^2 + k^2 + O(k^4) \right) . \tag{2.3}$$

The coefficients can be expressed in terms of moments of the spectral density $\rho(\mu)$ via

$$Z_{\mathrm{R}} = Z \frac{\gamma_2^2}{\delta_2} , \qquad \frac{M_{\mathrm{R}}^2}{M^2} = \frac{\gamma_2}{\delta_2} , \tag{2.4}$$

where $M$ is the mass gap and $\gamma_2$ and $\delta_2$ are the moments

$$\gamma_2 = M^2 \int d\mu \, \frac{\rho(\mu)}{\mu^2}, \qquad \delta_2 = M^4 \int d\mu \, \frac{\rho(\mu)}{\mu^4} \,. \tag{2.5}$$

Our normalization for the spectral density is such that

$$G(k) = Z \int_0^\infty d\mu \frac{\rho(\mu)}{\mu^2 + k^2} \,, \tag{2.6}$$

with the one-particle contribution given by $\rho^{(1)}(\mu) = \delta(\mu - M)$. (To avoid irrelevant complications we assume that the spectrum of the theory contains a doublet of stable particles of mass $M$.)

The intrinsic or renormalized 4-point coupling is an important measure for the interaction strength of a QFT. A conventional definition is

$$g_{\mathrm{R}} = -\frac{M_{\mathrm{R}}^2}{4G(0)^2} \sum_{a,b} G^{aabb}(0,0,0,0) \,, \tag{2.7}$$

where $G^{abcd}$ is defined through the Fourier transform of the connected 4-point function:

$$\int \prod_{j=1}^4 \left[ d^2 x_j e^{i k_j x_j} \right] \langle S^{a_1}(x_1) S^{a_2}(x_2) S^{a_3}(x_3) S^{a_4}(x_4) \rangle_{conn}$$

$$= (2\pi)^2 \delta^{(2)}(k_1 + k_2 + k_3 + k_4) G^{a_1 a_2 a_3 a_4}(k_1, k_2, k_3, k_4) \,. \tag{2.8}$$

The coupling $g_{\mathrm{R}}$ can then be written as

$$g_{\mathrm{R}} = -\frac{2\gamma_4}{\gamma_2 \delta_2} \tag{2.9}$$

where $\gamma_4$ is defined through

$$G^{a_1 a_2 a_3 a_4}(0,0,0,0) = \frac{Z^2 \gamma_4}{M^6} \left( \delta^{a_1 a_2} \delta^{a_3 a_4} + \delta^{a_1 a_3} \delta^{a_2 a_4} + \delta^{a_1 a_4} \delta^{a_2 a_3} \right) \,. \tag{2.10}$$

In ref. [7] we computed the moments and coupling within the form factor approach in a certain truncation, and in Appendix D we present an improved approximation.

We also consider the two-point function of the Noether current $J_\mu$:

$$\int d^2x \, e^{ikx} \langle J_\mu(x) J_\nu(0) \rangle = C\delta_{\mu\nu} + \frac{I(k)}{k^2} \left( k_\mu k_\nu - k^2 \delta_{\mu\nu} \right) .$$ 

(2.11)

Here $C$ is the (regularization dependent) coefficient of a possible contact term. Only the coefficient $I(k)$ of the transversal part is physical. It vanishes at zero momentum due to the assumed mass gap. The infinite momentum limit on the other hand is model dependent and can be finite or infinite. For the O(2) model it is determined in Section 2.2.

## 2.2 Integrability and bootstrap S-matrix

A first hint why the O(2) model (with classical Lagrangian (2.1) for $n = 2$) might be quantum integrable stems from the observation that the known bootstrap S-matrix of the O($n$), $n \geq 3$, models has a smooth $n \to 2$ limit [51]. Here we record this limit and also outline the relation to other integrable models.

Assuming the spectrum of the model consisted of an O($n$) vector multiplet of massive particles the exact S-matrix of the $n \geq 3$ models was found by bootstrap methods [52]. For later use we adopt the projector decomposition

$$S_{ab}^{cd}(\theta) = S_0(\theta) \, (P_0)_{ab}^{cd} + S_1(\theta) \, (P_1)_{ab}^{cd} + S_2(\theta) \, (P_2)_{ab}^{cd},$$

(2.12)

where

$$S_0(\theta) = \frac{\theta + i\pi}{\theta - i\pi} \, S_1(\theta) \,, \qquad S_1(\theta) = \frac{(n-2)\theta + 2\pi i}{(n-2)\theta - 2\pi i} \, S_2(\theta) \,,$$

$$S_2(\theta) = -\exp\left\{ 2i \int_0^\infty \frac{d\omega}{\omega} \sin\omega\theta \left[ \frac{e^{-\pi\omega} + e^{-2\pi\frac{\omega}{n-2}}}{1 + e^{-\pi\omega}} \right] \right\} .$$

(2.13)

The projectors are those on the O($n$) singlet, vector, and symmetric traceless tensors, i.e.

$$(P_0)_{ab}^{cd} = \frac{1}{n}\delta^{ab}\delta^{cd} \,,$$

$$(P_1)_{ab}^{cd} = \frac{1}{2}\left( \delta^{ac}\delta^{bd} - \delta^{bc}\delta^{ad} \right) ,$$

$$(P_2)_{ab}^{cd} = \frac{1}{2}\left( \delta^{ac}\delta^{bd} + \delta^{bc}\delta^{ad} \right) - \frac{1}{n}\delta^{ab}\delta^{cd} \,.$$

(2.14)

Contact to the Lagrangian (2.1) can be made through quantum conserved charges of higher spin that prevent particle production. Under mild extra assumptions Polyakov [41]

6

and Lüscher [33] have shown the existence of such respectively local and nonlocal higher spin conserved charges. The latter in particular anticipate [33] a Yangian structure and entail the factorization equations that dictate the S-matrix.

Much less is known about the O(2) model. A simple observation is that the amplitudes (2.13) have a smooth $n \to 2$ limit. This suggests that the O(2) model might likewise be integrable and that its spectrum consists of a single O(2) doublet of massive particles whose scattering is described by the $n \to 2$ limit of the S-matrix (2.12). Although taking this formal $n \to 2$ limit is not convincing in itself, the conclusion is corroborated by the KT theory [28] of the XY model and its reformulation in the context of the Sine-Gordon theory [1]. Before turning to the KT theory we thus briefly digress on the Sine-Gordon (SG) model. Its Lagrangean can be written as

$$\mathcal{L}^{\mathrm{SG}} = \frac{1}{2}\partial_\mu\phi\partial_\mu\phi + \frac{\alpha}{\beta^2}\left[1 - \cos(\beta\phi)\right], \tag{2.15}$$

where $\alpha$ has mass dimension 2 and $\beta$ is the dimensionless SG coupling. It is also integrable and its spectrum and S-matrix was also found in [52]. The spectrum depends on $\beta$ in a complicated way but it becomes simple for the range $8\pi > \beta^2 > 4\pi$ when it is free of bound states and consists of a single O(2) vector of massive particles. In terms of $\nu = \frac{8\pi}{\beta^2} - 1$ this corresponds to $0 < \nu < 1$, and the S-matrix in this range can be written in the projector form (2.12), with $n = 2$, where now

$$S_0(\theta|\nu) = \frac{\mathrm{sh}\frac{\nu}{2}(i\pi + \theta)}{\mathrm{sh}\frac{\nu}{2}(i\pi - \theta)}\, S_2(\theta|\nu)\,, \qquad S_1(\theta|\nu) = -\frac{\mathrm{ch}\frac{\nu}{2}(i\pi + \theta)}{\mathrm{ch}\frac{\nu}{2}(i\pi - \theta)}\, S_2(\theta|\nu)\,,$$

$$S_2(\theta|\nu) = -\exp\left\{2i\int_0^\infty \frac{d\omega}{\omega}\sin\omega\theta\,\frac{\sinh\frac{\pi\omega(1-\nu)}{2\nu}}{2\cosh\frac{\pi\omega}{2}\sinh\frac{\pi\omega}{2\nu}}\right\}. \tag{2.16}$$

Note that in the $\beta^2 \to 8\pi$ ($\nu \to 0$) limit the SG S-matrix coincides with the $n \to 2$ limit of the O($n$) S-matrix.

Finally, in the vicinity of $\beta^2 = 8\pi$ the SG model can also be related to a fermionic model [8] formulated in terms of a two-component Dirac fermion. It has a manifest SU(2) symmetry and is a variant of the chiral Gross-Neveu model with four-fermion interaction. The existence of this fermionic model sheds some light on the symmetry enhancement in the O(2) model discussed in Section 3. For the details, however, the difference between $SU_{-1}(2)$ and $SU(2)$ is crucial; c.f. the discussion at the end of Section 3.2.

The relation to these other integrable QFTs can in particular be used to determine the infinite momentum limit of the current two-point function $I(k)$ in (2.11). In the O(2) model

7

the limit is finite and exactly calculable. One way of computing $I(\infty)$ is by noting that it coincides with the coefficient of the Schwinger term in the current-current commutator. This commutator can be evaluated in the SG language using canonical quantization, and yields

$$I(\infty) = \frac{2}{\pi}\,. \tag{2.17}$$

The same result can be obtained using the relation to the before mentioned two-fermion model. Here, referring to the asymptotic freedom of the model in the fermion coupling constant, only a simple free fermion calculation has to be done.

## 2.3 Standard lattice action and KT theory

The standard lattice action of the XY model is

$$S_{\mathrm{XY}} = K \sum_{x,\mu} \left[ 1 - \cos\left( \varphi(x) - \varphi(x + \hat{\mu}) \right) \right]. \tag{2.18}$$

We denote the inverse temperature (inverse of the bare coupling) of the XY model by $K$ to avoid confusion with the SG coupling $\beta$.

This model has a high temperature phase at small $K$ with exponential decay of correlations; it has been shown rigorously [17] that at low temperature (large $K$) the correlations decay only like a power of the distance. The exponential decay disappears therefore at a finite critical value $K_c$; this is the famous KT transition predicted by Kosterlitz and Thouless [28]. They argued that at not too small values of $K$ typical configurations of the model can be described as a combination of 'smooth', topologically trivial configurations (spin waves) and a gas of vortices (of integer topological charge). The vortices have a logarithmic interaction and therefore form essentially a two-dimensional Coulomb gas, which has a transition from a high temperature phase with Debye screening to a low temperature dipole phase without screening. In the KT picture the transition is therefore described as 'vortex condensation'. A different perspective of this kind of phase transition was proposed in [38] according to which it is driven by the change from instanton-like defects (vortices) to super-instantons dominating at low temperatures.

Fröhlich and Spencer [17] established a rigorous version of the correspondence between the XY model and a type of Coulomb gas and used rigorous arguments inspired by the renormalization group (grouping of charges into neutral 'molecules') to show the absence of screening in this gas at low temperature.

Kosterlitz and Thouless employed heuristic energy-entropy considerations to show that in the transition region only vortices of topological charge $\pm 1$ are important and higher vortices can be neglected. It is easy to see that this system (spin waves and Coulomb gas with unit charge vortices only) is exactly equivalent to the SG model. In ref. [1] it was argued that the extremal SG fixed point $\beta^* = \sqrt{8\pi}$, $\alpha^* = 0$ is appropriate to describe the KT phase transition. The renormalizability of the SG model around this point was explicitly demonstrated up to two-loop order in a double expansion in $\alpha$ and $\delta = \frac{\beta^2 - 8\pi}{8\pi}$.

## 3. Bootstrap description and symmetry enhancement

Here we detail on the proposed bootstrap S-matrix, the associated quantum group structure and its implications for the form factors and the operator classification.

### 3.1 $SU_{-1}(2)$ invariance of the S-matrix

The candidate S-matrix for the XY QFT can be rewritten as

$$S_{ab}^{cd}(\theta) = S_2(\theta) \left[ \delta_a^d \delta_b^c + \frac{\theta}{i\pi - \theta} \delta_{ab} \delta^{cd} \right] , \qquad S_2(\theta) = \frac{\Gamma\left(\frac{1}{2} + \frac{\theta}{2\pi i}\right) \Gamma\left(-\frac{\theta}{2\pi i}\right)}{\Gamma\left(\frac{1}{2} - \frac{\theta}{2\pi i}\right) \Gamma\left(\frac{\theta}{2\pi i}\right)} . \qquad (3.1)$$

The S-matrix (3.1) satisfies the usual S-matrix postulates with the charge conjugation matrix $C_{ab} = \delta_{ab}$ and normalization $S_{ab}^{cd}(0) = -\delta_a^d \delta_b^c$. Note the nontrivial limit

$$S_{ab}^{cd}(\pm\infty) = \delta_a^d \delta_b^c - \delta_{ab} \delta^{cd} , \quad S(\pm\infty)^2 = \mathbb{1} . \qquad (3.2)$$

The symmetry group of the massive O(2) model is of course O(2), as far as the Lagrangian and the functional measure is concerned. The proposal (3.1) however entails that on the level of the S-matrix and the scattering states a symmetry enhancement takes place, in that on them a nonabelian symmetry operates. In view of the known $\mathcal{U}_q(su(2))$ quantum group symmetry of the Sine-Gordon S-matrix [42] and the identification $q = -e^{i\pi(-1+8\pi/\beta^2)}$, one expects the symmetry to be $\mathcal{U}_{-1}(su(2))$. As a Lie algebra this is the same as $\mathcal{U}_1(su(2)) = su(2)$, but the comultiplication in $\mathcal{U}_{-1}(su(2))$ differs from that in $su(2)$. We refer to Appendix A for some basic definitions and our conventions on $\mathcal{U}_q(su(2))$. To simplify the notation we shall write $SU_{-1}(2)$ for $\mathcal{U}_{-1}(su(2))$ from now on.

The easiest way to see the $SU_{-1}(2)$ invariance of the S-matrix (3.1) is to perform a projector decomposition. Defining $\check{S}^{cd}_{ab}(\theta) := S^{dc}_{ab}(\theta)$ (so that $\check{S}(0) = -\mathbb{1}$) it takes the form

$$\check{S}(\theta) = S_2(\theta) \left[ \frac{i\pi + \theta}{i\pi - \theta} P_0 + P_1 \right] , \qquad \text{with}$$

$$(P_0)^{cd}_{ab} = \frac{1}{2}\delta_{ab}\delta^{cd} , \qquad (P_1)^{cd}_{ab} = \delta^c_a\delta^d_b - \frac{1}{2}\delta_{ab}\delta^{cd} . \tag{3.3}$$

Here $P_0 P_1 = 0 = P_1 P_0$ and $P_0 + P_1 = \mathbb{1}$. Moreover $P_0$ and $P_1$ are the projectors onto the irreducible singlet and triplet representation of $SU_{-1}(2)$, respectively. For comparison let us note that the $SU(2)$ invariant S-matrix can likewise be written in the form (3.3), but the projectors are given by

$$SU(2): \qquad (P_0)^{cd}_{ab} = \frac{1}{2}\left(\delta^c_a\delta^d_b - \delta^d_a\delta^c_b\right) , \qquad (P_1)^{cd}_{ab} = \frac{1}{2}\left(\delta^c_a\delta^d_b + \delta^d_a\delta^c_b\right) . \tag{3.4}$$

The S-matrices (3.1) and (3.4) are of course also invariant under the usual real O(2) transformations. It is often advantageous to diagonalize this action by means of a unitary basis transformation

$$U = \frac{1}{\sqrt{2}} \begin{pmatrix} 1 & i \\ 1 & -i \end{pmatrix} = U_\alpha{}^a , \tag{3.5}$$

where we use Greek letters $\alpha, \beta, \ldots \in \{\pm\}$ to label the components in the new basis. Explicitly $S^{\gamma\delta}_{\alpha\beta}(\theta) := U_\alpha^a U_\beta^b S^{cd}_{ab}(\theta) U_c^\gamma U_d^\delta$, which now has $C_{\alpha\beta} = \delta_{\alpha+\beta,0}$ as its charge conjugation matrix. Written in matrix form one finds the familiar pattern for (3.3)

$$S(\theta) = \begin{pmatrix} S_2 & 0 & 0 & 0 \\ 0 & S_T & S_R & 0 \\ 0 & S_R & S_T & 0 \\ 0 & 0 & 0 & S_2 \end{pmatrix} , \qquad S_T(\theta) = \frac{\theta}{i\pi - \theta} S_2(\theta) , \quad S_R(\theta) = \frac{i\pi}{i\pi - \theta} S_2(\theta) , \tag{3.6}$$

where the rows and columns refer to the $(++, +-, -+, --)$ ordering. For the $SU(2)$ invariant S-matrix only the sign of $S_T$ would be flipped, which in view of the previous discussion however indicates a very different group theoretical structure. Concretely the $SU_{-1}(2)$ invariance of (3.6) amounts to

$$\Sigma_\pm \check{S}(\theta) = \check{S}(\theta)\, \Sigma_\pm , \quad \text{with} \quad \Sigma_+ = \Sigma_-^T = i \left( \begin{array}{c|ccc} 0 & & & \\ -1 & & 0 & \\ 1 & & & \\ \hline 0 & -1 & 1 & 0 \end{array} \right) , \tag{3.7}$$

and $\Sigma_\pm$ representing the 'raising and lowering' operators of $SU_{-1}(2)$.

## 3.2 Form factors: O(2) versus $SU_{-1}(2)$ covariance

Form factors in this context are matrix elements of some local quantum field between the vacuum and a multi-particle scattering state. They can in principle be computed from a recursive system of functional equations defined largely in terms of the given bootstrap S-matrix. Since the S-matrix has the enhanced $SU_{-1}(2)$ symmetry it is natural to ask whether the associated functional equations are likewise covariant. Unlike the situation in other models this turns out to be *not the case* automatically, but it rather hinges on the values of certain statistics phases. Since this is a novel feature we briefly outline the general structure of the form factor equations in the O(2) bootstrap theory here. Details are relegated to Appendix A. Explicit results for some operators of interest are given in the next section and Appendices B and C.

The form factors are tensors with respect to the obvious (real) action of O(2) rotations. As with the S-matrix it convenient to diagonalize this action by the unitary transformation (3.5). We write $f_{\alpha_n \dots \alpha_1}(\theta_n, \dots, \theta_1)$ for the components of some $n$-particle form factor in this "charged basis". The terminology is motivated by the fact that under a $U(1)$ transformation a form factor picks up a phase $e^{ie\varphi}$, where $e := \alpha_n + \dots + \alpha_1$ plays the role of the $U(1)$ charge. Equivalently $e$ is the weight with respect to the Cartan subalgebra generator of $SU_{-1}(2)$. A form factor (of an operator) of Lorentz spin $s$ should also have the homogeneity property

$$f_{\alpha_n \dots \alpha_1}(\theta_n + u, \dots, \theta_1 + u) = e^{su} \, f_{\alpha_n \dots \alpha_1}(\theta_n, \dots, \theta_1) \,. \tag{3.8}$$

For a fixed particle number $n$ a form factor then has to satisfy the functional equations

$$f_{\alpha_n \dots \alpha_1}(\theta_n, \dots, \theta_2, \theta_1) = S^{\delta \ \gamma}_{\alpha_2 \alpha_1}(\theta_{21}) \, f_{\alpha_n \dots \alpha_3 \gamma \delta}(\theta_n, \dots, \theta_1, \theta_2) \,, \tag{3.9a}$$

$$f_{\alpha_n \dots \alpha_1}(\theta_n + 2\pi i, \theta_{n-1}, \dots, \theta_2, \theta_1) = \Gamma^{\delta}_{\alpha_n} \, f_{\alpha_{n-1} \dots \alpha_1 \delta}(\theta_{n-1}, \dots, \theta_1, \theta_n) \,. \tag{3.9b}$$

In the second Eq. the shift by $2\pi i$ is to be understood in the sense of analytical continuation and $\Gamma^{\beta}_{\alpha}$ is a constant matrix on whose role we elucidate below. First note that the system (3.9) decomposes into decoupled sectors with fixed $U(1)$ charge $e \in \{n, n-2, \dots, -n+2, -n\}$ and dimension $n!/n_-!(n-n_-)!$, where $n_- = (n-e)/2$ is the number of '$-$' labels in $(\alpha_n, \dots, \alpha_1)$. Correspondingly the matrix $\Gamma$ is diagonal in this basis but may be different in different charge sectors

$$\Gamma^{\beta}_{\alpha} = \eta_{\alpha}(e) \, \delta^{\beta}_{\alpha} \,. \tag{3.10}$$

The phases $\eta_\alpha(e)$ can be thought of as statistics phases describing the relative statistics of the (quasilocal) operator whose form factors are considered and the field that generates the scattering states in a Haag-Ruelle type scattering theory [36]. See e.g. [29] for some simple examples. Iterating (3.9b) and employing the analyticity in $u$ of (3.8) one finds the following *spin-statistics* relation

$$\eta_-(e)^{n_-} \, \eta_+(e)^{n-n_-} = e^{2\pi i s} \ . \tag{3.11}$$

A further condition arises if the underlying operator is hermitian. From $f_{\alpha_n \dots \alpha_1}(\theta_n, \dots, \theta_1)^*$ $= f_{-\alpha_1 \dots -\alpha_n}(\theta_1^* + i\pi, \dots, \theta_n^* + i\pi)$ one obtains

$$\eta_\alpha(e)\eta_{-\alpha}(-e)^* = 1 \ . \tag{3.12}$$

If only O(2) invariance is assumed no further constraints exist and the phases $\eta_\alpha(e)$ are part of the specification of a field operator in the bootstrap framework. Collectively they encode the information about the super selection structure of the theory. Since the first Eq. in (3.9) is covariant also with respect to the larger nonabelian $SU_{-1}(2)$ symmetry, it is natural to ask whether or not also the second Eq. is covariant for a suitable choice of the phases. The covariance requirement links the charge $e$ sector with the $e \pm 2$ sectors. It can be seen to entail an overdetermined set of relations for the phases $\eta_\alpha(e)$, – which turn out to be self-consistent. The requirement of quantum group covariance thus determines all phases $\eta_\alpha(e)$ essentially uniquely; c.f. Appendix A. For $n \le 4$ one finds explicitly:

$$n = 2 : \quad \eta_+(2) = -\eta_\pm(0) = \eta_-(-2) \ ,$$
$$n = 3 : \quad \eta_+(3) = \mp\eta_\pm(1) = \pm\eta_\pm(-1) = \eta_-(-3) \ ,$$
$$n = 4 : \quad \eta_+(4) = -\eta_\pm(2) = \eta_\pm(0) = -\eta_\pm(-2) = \eta_-(-4) \ . \tag{3.13}$$

Generally, for fixed $n$, the relative signs are given by $\eta_\alpha(e) \sim \exp\frac{i\pi}{2}(e - n\alpha)$. Of course the actual phases solving (3.13) must be chosen $n$-independent.

Let us illustrate the use of these relations in the charge $e = 1$ sector (where only the odd particle form factors are nonzero). We can take $\eta_\pm(1) = e^{\pm 2\pi i s}$ as the solution of (3.11). Then (3.12) fixes $\eta_\pm(-1) = e^{\mp 2\pi i s}$. If we now in addition require that the field underlying these form factors is quantum group covariant, the $e = \pm 1$ sectors are linked by (3.13), e.g. for $n = 3$. This yields the condition $e^{\mp 4\pi i s} = -1$, and we conclude: $s = 1/4 \, \mathrm{mod} \, 1/2$. In words, *an O(2) doublet field that is in addition quantum group covariant can only have*

*Lorentz spin* $s = 1/4 \bmod 1/2$. If we had started from the $SU(2)$ invariant S-matrix (3.4) instead, no relative signs in (3.13) would have occurred, and an $SU(2)$ doublet of O(2) charge $e = \pm 1$ was forced to have Lorentz spin $s = 1/2 \bmod 1/2$, as expected.

Next we proceed to the residue equations which link an $n$-particle form factor to an $n-2$ particle form factor. Consistency requires that the inverse of the matrix $\Gamma^\beta_\alpha$ appears on the right hand side, irrespective of its concrete form. In the charged basis the precise formula is given in (A.9). For generic phases (A.9) will only be O(2) covariant. Concretely this means that an $n$-particle form factor of $U(1)$ charge $e$ is linked to an $n$–2 particle form factor with the same $U(1)$ charge. For the choice (3.13) ensuring the $SU_{-1}(2)$ covariance of (3.9) one expects that also (A.9) is quantum group covariant, which indeed turns out to be the case. Since all form factor Eqs then are covariant a quantum group transformation will map one solution into another solution, where "solution" actually means a sequence of functions whose members are linked by the (A.9). Suitable sequences should correspond to (local) quantum fields in the O(2) model. We thus find that field operators whose statistics phases enjoy the specific relation (3.13) form multiplets with respect to the quantum group action. Clearly one can concentrate on the multiplets transforming irreducibly; the multiplet and the associated form factor sequence will then be characterized by an isospin quantum number stemming from the representation theory of $SU_{-1}(2)$. In appendix A we list the irreducible multiplets for $n \leq 4$.

We can summarize the situation as follows: The functional equations characterizing the form factors are O(2) invariant and decompose into decoupled sectors with fixed $U(1)$ charge $e$. In each sector statistics phases $\eta_\alpha(e)$ enter that are part of the specification of a field operator (or of an O(2) multiplet thereof) in the bootstrap framework. In addition operators from *different* charge sectors whose statistics phases enjoy the particular relation (3.13) are members of an (irreducible) multiplet with respect to the nonabelian quantum group $SU_{-1}(2)$. The existence of these multiplets is a nontrivial prediction of the bootstrap formulation.

As remarked earlier there exists a (non-rigorous) transformation of the O(2) model into a fermionic model with a manifest SU(2) invariance, for which the natural candidate S-matrix is (3.4), i.e. that of the SU(2) chiral Gross-Neveu model. As with the O(2) – Sine-Gordon correspondence we expect that both systems share *subsets* of fields with identical correlation functions. An interesting one-to-one correspondence of the fields however is unlikely. To see this let us discuss the relation between the bootstrap systems based on the $SU_{-1}(2)$ invariant S-matrix (3.1) and the $SU(2)$ S-matrix (3.4) in more

detail: In the charged basis the mapping

$$|\theta_n, \ldots, \theta_1\rangle_{\alpha_n \ldots \alpha_1} \; \longrightarrow \; \prod_{j=1}^{n} (\alpha_j)^j \, |\theta_n, \ldots, \theta_1\rangle_{\alpha_n \ldots \alpha_1} \,, \tag{3.14}$$

maps states whose exchange relations are governed by the $SU(2)$ S-matrix (3.4) onto those whose exchange relations are governed by the $SU_{-1}(2)$ S-matrix (3.1), and also 'untwists' the non-trivial comultiplication of $SU_{-1}(2)$ [43]. However (3.14) does not induce an interesting correspondence of the form factor sequences. For example if the $SU(2)$ statistics phases are taken to be unity, the mapping (3.14) induces $\eta_\alpha^{\text{induced}}(e) = e^{i\pi(e - n\alpha)/2}$ for the $SU_{-1}(2)$ bootstrap system. This flips sign under $n \to n - 2$ while the statistics phases of a sequence acceptable for describing a $SU_{-1}(2)$ covariant field operator of course must be $n$-independent. Mathematically one can set up a correspondence between solutions of the form factor equations based on the $SU(2)$ and the $SU_{-1}(2)$ S-matrix. One way of doing this is to substitute the respective S-matrices into the Bethe Ansatz inspired integral formulae of [43, 3]. However this correspondence will in general *not preserve* the spin, the statistics phases, or even the covariance under the global symmetry group. One must conclude that there is no physically interesting one-to-one correspondence between the field content of the bootstrap systems based on the $SU(2)$ and on the $SU_{-1}(2)$ S-matrix.

### 3.3 Spin, Parafermion and Current form factors for $n \leq 4$

With these preparations at hand we now seek to determine the form factors of the Noether current $J_\mu = \frac{1}{g^2}(S^1 \partial_\mu S^2 - S^2 \partial_\mu S^1)$ and the basic Spin field $S^a$, $a = 1, 2$. The latter is an O(2) doublet and carries Lorentz spin $s = 0$. From the discussion following (3.13) we conclude that it cannot be a quantum group doublet as well. We thus also search for the form factors of an additional *local* "parafermion" field that is a $SU_{-1}(2)$ doublet with Lorentz spin 1/4. (We shall comment on the relation to Smirnov's parafermion in the SG model [44] below.) Technically the construction of form factors for the Spin and the parafermion field is very similar. In order to treat both cases simultaneously we write $\Phi_s^a(x)$ for the renormalized field operators, with $s = 0, 1/4$, corresponding to the spin and the parafermion field, respectively. The objects of interest then are

$$\langle 0 | J_\mu(0) | \theta_n, \alpha_n; \ldots; \theta_1, \alpha_1 \rangle \;=\; -i\epsilon_{\mu\nu} \left( \sum_{j=1}^{n} p^\nu(\theta_j) \right) f_{\alpha_n \ldots \alpha_1}(\theta_n, \ldots, \theta_1) \,, \quad n \text{ even}, \tag{3.15}$$

$$\langle 0 | \Phi_s^\alpha(0) | \theta_n, \alpha_n; \ldots; \theta_1, \alpha_1 \rangle \;=\; f_{\alpha_n \ldots \alpha_1}^\alpha(\theta_n, \ldots, \theta_1) \,, \quad n \text{ odd}. \tag{3.16}$$

14

Here all components refer to the charged basis. The current form factors have charge $e = 0$ while that of $\Phi_s^\pm(x)$ have charge $e = \pm 1$. The prefactor in the current form factor ensures current conservation; the on-shell momenta are $p_0(\theta) = M\text{ch}\theta$, $p_1(\theta) = M\text{sh}\theta$. As always in the form factor bootstrap Eqs (3.15), (3.16) must be regarded as a "statement of intent". That is, the right hand is computed through the functional equation while the interpretation as the matrix elements aimed at on the left hand side has to be justified by additional considerations.

As input for the recursive functional equations the normalization of the starting members has to be fixed. For the current a preferred normalization stems from the fact that the associated Noether charge $Q$ should induce $O(2)$ rotations on the spins, i.e. $[Q, S^a] = i\epsilon_{ab}S^b$. For the 2-particle form factor this converts into

$$f_{+-}(\theta_2, \theta_1) = -f_{-+}(\theta_2, \theta_1) = \frac{2i}{\theta_2 - \theta_1 - i\pi} + \dots , \quad \theta_2 \to \theta_1 + i\pi , \qquad (3.17)$$

where the dots denote regular terms. Writing $f_{+-}(\theta_2, \theta_1) = f(\theta_2 - \theta_1)$ the function $f(\theta)$ has to satisfy the functional eqs $f(\theta) = S_2(\theta)f(-\theta)$ and $f(\theta + 2\pi i) = -f(-\theta)$, with $S_2(\theta)$ from (3.1). They can be solved in terms of the function

$$y(\theta) := \text{sh}\frac{\theta}{2}e^{\Delta(\theta)} ,$$

$$\Delta(\theta) := \int_0^\infty \frac{dt}{t} \frac{\text{ch}t(1 + i\theta/\pi) - 1}{(1 + e^t)\text{sh}t} , \qquad (3.18)$$

which enjoys the following properties

$$y(\theta) = S_2(\theta)y(-\theta) , \quad y(\theta + 2\pi i) = y(-\theta) ,$$

$$y(\theta)y(\theta + i\pi) = -\frac{\pi^{3/2}e^{\Delta(0)}}{\Gamma\left(\frac{1}{2} - \frac{\theta}{2\pi i}\right)\Gamma\left(\frac{\theta}{2\pi i}\right)} , \quad y(i\pi) = i . \qquad (3.19)$$

We also note

$$\Delta(0) = 0.304637 , \qquad \lim_{\theta \to +\infty}[\Delta(\theta) - \Delta(-\theta)] = \frac{i\pi}{2} . \qquad (3.20)$$

Taking into account the residue condition (3.17) one obtains

$$f_{+-}(\theta_2, \theta_1) = -f_{-+}(\theta_2, \theta_1) = i\frac{y(\theta_2 - \theta_1)}{\text{ch}\frac{\theta_2 - \theta_1}{2}} . \qquad (3.21)$$

With the 2-particle form factor explicitly known one can proceed to the 4-particle form factor. The formulas now get more involved and we defer the details to appendix B. The

Lorentz spin $s = 1$ is readily checked to be compatible with $SU_{-1}(2)$ covariance via (3.11) – (3.13). The (one-component) Noether current in the O(2) model is the neutral member of a hidden quantum group triplet [43], although the charge $e = \pm 2$ partners are nonlocal in the spin field.

For the $\Phi_s^\alpha(x)$ fields a natural normalization is

$$\langle 0 | \Phi_s^\alpha(0) | \theta, \beta \rangle = f_\beta^\alpha(\theta) = \delta_\alpha^\beta \, e^{\alpha s \theta} \,. \tag{3.22}$$

Proceeding to the 3-particle form factor we note that because of charge conservation and hermiticity there are only three independent components

$$f_{++-}^+(\theta_3, \theta_2, \theta_1) = f_1(\theta_1, \theta_2, \theta_3) = f_{--+}^-(\theta_3, \theta_2, \theta_1) \,,$$

$$f_{+-+}^+(\theta_3, \theta_2, \theta_1) = f_2(\theta_1, \theta_2, \theta_3) = f_{-+-}^-(\theta_3, \theta_2, \theta_1) \,,$$

$$f_{-++}^+(\theta_3, \theta_2, \theta_1) = f_3(\theta_1, \theta_2, \theta_3) = f_{+--}^-(\theta_3, \theta_2, \theta_1) \,. \tag{3.23}$$

The general 3-particle residue equation (A.9) in the charge $e = \pm 1$ sectors

$$\frac{i}{2} \mathrm{res}_{\theta_{3,2}=i\pi} f_{\alpha_3 \alpha_2 \alpha_1}^\alpha(\theta) = \delta_{\alpha_3 + \gamma} \left[ \eta_\gamma(e)^{-1} S_{\alpha_2 \alpha_1}^{\beta \, \gamma}(\theta_{21}) - \delta_{\alpha_2}^\gamma \delta_{\alpha_1}^\beta \right] f_\beta^\alpha(\theta_1) \,, \tag{3.24}$$

thus translates into

$$f_k(u, v, \theta) \approx \frac{2i}{u - v - i\pi} W_k(v - \theta) \,, \qquad u \to v + i\pi \,, \tag{3.25}$$

where with $\eta := \eta_+(1) = e^{2\pi i s}$ and the notation from (3.6)

$$W_1(\theta) = -\eta S_R(\theta) \,, \quad W_2(\theta) = 1 - \eta S_T(\theta) \,, \quad W_3(\theta) = 1 - \eta^{-1} S_2(\theta) \,. \tag{3.26}$$

These functional equations can be solved for generic $s$, the solution is described in appendix C. For the spin field $s = 0$ fixes our candidate form factors. For the parafermion field we know that $SU_{-1}(2)$ covariance (regardless of irreducibility) requires $s = 1/4$. (The specific construction used in appendix C removes the additive mod $1/2$ ambiguities). As explained in appendix A the condition that the parafermion field (and hence its form factors) transform irreducibly as a isospin $1/2$ doublet requires in addition

$$\zeta(\theta_3, \theta_2, \theta_1) := f_1(\theta_3, \theta_2, \theta_1) - f_2(\theta_3, \theta_2, \theta_1) + f_3(\theta_3, \theta_2, \theta_1) \overset{!}{=} 0 \,. \tag{3.27}$$

For the solution constructed in Appendix C, $\zeta(\theta_3, \theta_2, \theta_1)$ can be shown to be proportional to $\eta^2 + 1$, so that $s = 1/4$ also entails the desired irreducible transformation law.

So far we didn't say anything about the local structure of the parafermion field $\Phi^\alpha_{1/4}(x)$ supposed to underly the above solution of the form factor equations. We can address this point by employing a result by Smirnov [44] on the existence of parafermionic fields in the Sine-Gordon model. Smirnov's fields have well defined exchange relations of the form $\Psi_a(x)\Psi_b(y) = S^{cd}_{ab}(\pm\infty)\Psi_d(y)\Psi_c(x)$, for $\pm x^1 > \pm y^1$, where $x^1, y^1$ are the space components of $x, y$ in a fixed Lorentz frame. For generic Sine-Gordon coupling $\beta$ these fields are nonlocal because the two limiting S-matrices are distinct. From the analysis of the form factors of the energy momentum tensor one can see that our parafermion field is the $\beta^2 \to 8\pi$ limit of Smirnov's field. But thanks to (3.2) it is now a *local* field. Indeed for the charged components the exchange relations assume the simple form

$$\Phi^\pm_{1/4}(x)\Phi^\pm_{1/4}(y) = \Phi^\pm_{1/4}(y)\Phi^\pm_{1/4}(x),$$
$$\Phi^+_{1/4}(x)\Phi^-_{1/4}(y) = -\Phi^-_{1/4}(y)\Phi^+_{1/4}(x), \tag{3.28}$$

for *all* spacelike separated points $x, y$. Likewise the transformation properties under the quantum group change qualitatively. As analyzed by several authors [44, 30, 16] in general a dynamical quantum group symmetry of the S-matrix acts in a nonlocal way on the field operators. In contrast the field $\Phi^\alpha_{1/4}(x)$ transforms nicely as an irreducible $SU_{-1}(2)$ doublet. The situation is thus reminiscent of the Ising model, which can be viewed as the $n = 1$ case of (2.1). There both the spin and the fermion are local fields of Lorentz spin 0 and 1/2, respectively. Both are relatively non-local but generate equivalent sets of scattering states. Though in the absence of a field theoretical construction of the parafermion field it is difficult to examine this point, we expect the interplay between the spin and the parafermion field in the XY QFT to be analogous.

17

# 4. Lattice computations

## 4.1 General setup

For the lattice regularization we consider a square lattice with action

$$S = -K \sum_{x,\mu} S(x) \cdot S(x + \hat{\mu}) \,, \tag{4.1}$$

where $S(x) \cdot S(x) = \sum_a S^a(x) S^a(x) = 1$. Solving the constraint with $S^1(x) = \cos \varphi(x)$, $S^2(x) = \sin \varphi(x)$ the action reduces to the standard XY lattice action Eq. (2.18). The correlation functions are defined as in the continuum theory except that the spatial integrals are replaced by discrete sums. There is an enormous literature, both on numerical simulations of the XY model [19] and on its high temperature expansion [10, 40]. Presently the best numerical estimate of the critical point for the standard action is [21]

$$K_c = 1.1199(1) \,. \tag{4.2}$$

Previous numerical investigations mostly concentrated on the comparison with the KT theory. We will outline the aspects relevant here and some refinements in Section 6.1. Our main goal however is to compare the continuum limit of the XY model with the O(2) bootstrap theory.

In the rest of this section we collect some general information on our simulations and continue with detailed discussions of the measurement of various observables in Sections 5 and 6. All numerical simulations were done on an $L \times T$ lattice with periodic boundary conditions in each direction. During the entire investigation two independently written programs were employed and many cross checks were made. Both used multi-cluster updating. The Ising spins are embedded like in Wolff's single cluster algorithm [50]; the resulting Ising model is then updated with a generalization of the Swendson-Wang [46] multi-cluster algorithm. In one application of the program each run started from a random configuration and consisted of a large number of sweeps of which a large initial proportion were used solely for equilibration. In another application after initial equilibration the final configuration of the run was stored and read in for the starting configuration of the next run. In most cases the observables were measured using improved (cluster) estimators. The final data sample of the many runs was averaged and the error was computed using the jack-knife method.

Since we aim at achieving high precision, for many quantities to an accuracy of $< 1\%$, a considerable source of concern to us was the random number generator (RNG). Indeed at an initial stage of this project we found that results obtained by various RNGs could differ by many standard deviations. We thus subjected the RNGs to several tests, specific to the model and the quantities considered here. The results are reported in Appendix E.

Numerical simulations of course are restricted to work in finite volume. In the next two subsections we therefore discuss finite volume effects, first in the continuum and then on the lattice.

## 4.2 Finite volume effects in the continuum

If a continuum QFT is confined in a box the physical observables will depend on the geometry and boundary conditions. Consider first the mass $m(L)$ of the 1-particle state on a cylinder of circumference $L$. Lüscher [32] has shown that in a theory without a "three–point coupling" of this particle to itself or to any other single–particle state, for large physical volumes $z = ML \gg 1$ the finite volume dependence of the mass is given by:

$$D(z) \equiv \frac{m(L) - M}{M} = \frac{1}{\pi} \int_0^\infty dt\, e^{-z \cosh t} \cosh(t) f(t) + \ldots, \tag{4.3}$$

where $f(t)$ is the forward scattering amplitude at an off–shell point. Thus in these models the infinite volume limit is approached rapidly at a rate $\sim \exp(-z)$ (from above if $f(0) > 0$).

More explicitly in the O$(n)$ sigma-models the amplitude $f$ is given by

$$f(t) = n - \frac{1}{2n} \left[ 2S_0(\theta) + n(n-1)S_1(\theta) + (n+2)(n-1)S_2(\theta) \right]_{\theta=t+i\pi/2}. \tag{4.4}$$

With the proposed S-matrix (2.12), (3.1) of the O$(2)$ model one obtains

$$f(t) = 2 + \frac{2\pi^2}{t^2 + \pi^2/4} \left| \frac{\Gamma(3/4 - it/2\pi)}{\Gamma(1/4 - it/2\pi)} \right|^2, \tag{4.5}$$

in which case Eq. (4.3) results in

$$D(z) \sim 1.162475182 \frac{e^{-z}}{\sqrt{z}} \left[ 1 + 0.36432/z + O(1/z^2) \right]. \tag{4.6}$$

Next we consider the zero-momentum coupling in a square box of length $L$ in each direction. To get a feeling of the finite volume effects consider the expression for $g_R(L)$ in the leading order $1/n$ expansion [12]. One obtains

$$g_R(L) = g_R(\infty)[1 - \sqrt{8\pi}\, z^{A_4} e^{-z}(1 + O(1/z)) + \cdots]\,, \qquad (4.7)$$

with $A_4 = 1/2$. Although the $1/n$ expansion is not expected to be quantitatively applicable to $n = 2$, one might hope that the qualitative features are correct, in particular that the finite volume effects are exponentially suppressed and secondly that the exponent $A_4$ of the multiplicative power correction is independent of $n$. Some corroboration of this might come from investigating the finite volume effects in a square box in an effective Lagrangean framework similar to [32].

### 4.3 Finite volume effects in the lattice regularization

The particular lattice sizes used will be specified later, but they were generally selected to enable studies of finite size effects at fixed correlation length and vice versa, subject of course to restrictions due to the CPU power available to us.

For a coupling $g_R(K, L)$ depending on the bare coupling $K$ and size $L \times L$ which tends to $g_R$ in the continuum and infinite volume limits, we adopted the O($n$) definition

$$g_R(K, L) = \left(\frac{L}{\xi}\right)^2 \left[1 + \frac{2}{n} - \frac{\langle (\Sigma^2)^2 \rangle}{\langle \Sigma^2 \rangle^2}\right]\,, \qquad (4.8)$$

for $n = 2$, where $\Sigma^a = \sum_x S^a(x)$. In Eq. (4.8) and throughout Sect. 6, $\xi$ is taken to be

$$\xi = \frac{1}{2\sin(\pi/L)}\sqrt{\frac{G(0)}{G(k_0)} - 1}\,, \qquad (4.9)$$

where $k_0 = (2\pi/L, 0)$; c.f. ref. [15]. This correlation length converges in the thermodynamic limit to the second moment correlation length $1/M_R$. In this connection we would like to draw the reader's attention to a subtlety which is discussed at the end of Section 4 in ref. [7].

The Noether current on the lattice is defined by

$$J_\mu(x) = K\left\{S^1(x)\partial_\mu S^2(x) - S^2(x)\partial_\mu S^1(x)\right\}\,, \qquad (4.10)$$

where $\partial_\mu f(x) = f(x + \hat{\mu}) - f(x)$. Introducing its two point function as

$$J_{\mu\nu}(q|K, L) = \sum_x e^{iqx} \langle J_\mu(x) J_\nu(0) \rangle \,, \tag{4.11}$$

with $q = (q_1, q_2)$, the well-known Ward identity (for the standard action) reads

$$\sum_\mu \left( 1 - e^{iq_\mu} \right) J_{\mu\nu}(q|K, L) = \frac{K}{2} \left( 1 - e^{iq_\nu} \right) E(K, L) \,, \tag{4.12}$$

where the energy expectation $E$ is

$$E(K, L) = \sum_\mu \langle S(x) \cdot S(x + \hat{\mu}) \rangle \,. \tag{4.13}$$

Next we wish to define for a finite periodic lattice the counterpart of the transverse current correlation function $I(k^2)$ in (2.11). $J_{\mu\nu}$ can naturally be decomposed into 3 pieces ('transverse', 'longitudinal' and 'harmonic'), as discussed in [39]. The harmonic piece is concentrated at the origin in momentum space and has the value $J_{11}(0|K, L)$.

In the thermodynamic limit, because of the presence of a mass gap, $J_{\mu\nu}(q|K, L)$ will be a real analytic function; so it cannot contain any remnant of the harmonic piece (which would be proportional to a $\delta$ function). The longitudinal and the transverse parts have to go to the same limit as $q \to 0$ to avoid any non-analyticity at zero momentum. Being a contact term the value of $J_{\mu\nu}(0|K, L)$ has no physical meaning. For this reason, as explained already in Section 2.1, we define the transverse part in such a way that it vanishes at zero momentum in the thermodynamic limit. This suggests the definition

$$I((0, q_2)|K, L) := J_{11}((0, 0)|K, L) - J_{11}((0, q_2)|K, L) \,, \tag{4.14}$$

to which we shall refer as the SUB definition. It ensures $I(0) = 0$ at finite $L$ and $\xi$.

Another possible definition is suggested by the Ward identity, which for momenta of the form $q = (0, q_2)$ reads

$$I((0, q_2)|K, L) := \frac{K}{2} E(K, L) - J_{11}((0, q_2)|K, L) \,. \tag{4.15}$$

We can use (4.15) as an alternative definition for a lattice counterpart of $I(k^2)$ in (2.11), to which we shall refer to as the WARD definition. The normalization $I(0) = 0$ is then

only restored in the thermodynamic limit, but for numerical purposes the WARD version often is advantageous. To verify that (4.15) vanishes at $q = 0$ in the thermodynamic limit note that Eq. (4.12) also entails

$$J_{11}((q_1, 0)|K, L) = \frac{K}{2} E(K, L), \qquad \forall\, q_1 \neq 0. \tag{4.16}$$

Since $J_{11}((q_1, 0)|K, L)$ becomes a real analytic function of $q_1 \in [-\pi, \pi]$ for $L \to \infty$ Eq. (4.16) remains valid also for $q_1 = 0$ [39]. In the thermodynamic limit therefore the WARD and the SUB definitions are equivalent. In Section 6 we shall consider both options.

Unfortunately few rigorous results exist on finite size effects for $z = L/\xi(K, L) \gg 1$ on the lattice. In general we expect in the $O(n)$ models, for a large class of observables $\mathcal{O}$ and for fixed bare coupling $K$, the finite size effects to be either of the form

$$\mathcal{O}(K, L) = \mathcal{O}(K, \infty) + z^{A^{\mathcal{O}}} e^{-z} \left[ C_0^{\mathcal{O}}(K) + C_1^{\mathcal{O}}(K)\frac{1}{z} + O(1/z^2) \right] + \ldots, \tag{4.17}$$

or the same with $C_i^{\mathcal{O}}(K)$ replaced by $\mathcal{O}(K, \infty)C_i^{\mathcal{O}}(K)$. Here either the amplitudes $C_i^{\mathcal{O}}(K)$ or $\mathcal{O}(K, \infty)C_i^{\mathcal{O}}(K)$ are hoped to be almost constant for large correlation lengths. Further the dynamical assumption enters that the fall-off is $e^{-\alpha z}$ with $\alpha = 1$, as expected in the absence of two-particle bound states. Further it seems reasonable to expect $A^{\mathcal{O}}$ to depend only on the form of the observable and not on the dynamics e.g. not on $n$.

As mentioned earlier one can probably, for certain correlation functions, better justify these assumptions by performing a Feynman diagram analysis in the framework of an effective massive lattice field theory analogous Lüscher's in the continuum theory [32]. Here we only indicate some plausibility considerations based on the leading order in the lattice $1/n$ expansion (viewed as a summation of bubble diagrams). For the coupling this gives

$$n g_{\mathrm{R}}(K, L) = 2\triangle(0)/m_0^2 + O(1/n),$$

$$\text{with} \quad \triangle(0)^{-1} = \frac{1}{L^2} \sum_p (E_p + m_0^2)^{-2}, \qquad K = \frac{n}{L^2} \sum_p \left( E_p + m_0^2 \right)^{-1}. \tag{4.18}$$

Here $\xi = 1/m_0$ and the sums range over momenta $p_\mu = 2\pi\, n_\mu/L$, with $0 \leq n_\mu \leq L - 1$, $\mu = 1, 2$, and $E_p = 4\sum_\mu \sin^2 p_\mu/2$. For the current two point function the leading term is

$$J_{\mu\nu}(q|K, L) = \frac{n(n-1)}{2} \frac{1}{L^2} \sum_p \frac{\left[ e^{ip_\mu} - e^{-iP_\mu} \right]\left[ e^{-ip_\nu} - e^{iP_\nu} \right]}{\left[ E_p + m_0^2 \right]\left[ E_P + m_0^2 \right]}, \tag{4.19}$$

where $P = p + q$, and for the energy expectation it is

$$E(K, L) = \frac{n}{K} \frac{1}{L^2} \sum_p \frac{\sum_\mu \cos p_\mu}{E_p + m_0^2} . \tag{4.20}$$

Starting from these formulae one can study separately the finite volume effects and lattice artifacts in this approximation; the results confirm the before mentioned assumptions. We stress again the big qualitative difference between the finite volume effects and the lattice artifacts. Whereas the finite volume effects represent continuum physics and hence are expected to be structurally universal, the lattice artifacts are in general non-universal. In particular for the spin 2-point function one finds in this framework $A^{\mathcal{O}} = A_2 = -1/2$ for the exponent in (4.17), whereas for the current and $g_R$ we get $A^{\mathcal{O}} = A_4 = 1/2$. (Both the current 2-point function and $g_R$ depend linearly on spin 4-point functions and perhaps this accounts for the same exponent $A_4$.) If one does not wish to adopt this framework the exponents can be kept as fit parameters; c.f. Section 6.

## 4.4 Lattice artifacts

After the extrapolation to infinite volume has been performed, the results can be regarded as corresponding to a lattice O(2) action in infinite volume. The extrapolation to infinite correlation length is usually hampered by the lack of information about the rate of approach. Based on the Sine-Gordon description of the KT transition [1] one of us [4] has argued that for the XY model, say with standard action (4.1), the leading lattice artifacts are *calculable* from the continuum Sine-Gordon theory. This applies to observables like the S-matrix or the two-point function of the Noether current, where already at finite correlation length a preferred normalization exists. Implicit in this proposal is a certain degree of action-independence of the leading lattice artifacts, but at present it is not clear to which class of actions it applies. Later on we test this proposal for the standard action and the two observables mentioned.

Let $U_{\rm XY}(\xi)$ denote such an observable, where $\xi$ is the correlation length in lattice units and the dependence on other variables is suppressed. Then $U_{\rm XY}(\xi)$, computed e.g. with the standard action is predicted to be of the form [4]

$$U_{\rm XY}(\xi) = u_0 - \frac{u_1 \pi^2}{4(\ln \xi + u)^2} + O\big((\ln \xi)^{-4}\big). \tag{4.21}$$

Here $u_0$ is the continuum value and $u_1$ is the leading correction. The parameter $u$ is action-dependent but should not depend on the physical quantity considered. Note the

extremely slow decay $\sim 1/(\ln \xi)^2$. As explained in [4] the peculiar structure of the KT phase diagram allows one to relate both $u_0$ and $u_1$ to the continuum SG theory. Namely if $U_{\mathrm{SG}}(\nu)$ denotes the counterpart of the physical quantity considered in the continuum SG theory with coupling $\nu$ close to $\nu = 0$, then

$$U_{\mathrm{SG}}(\nu) = u_0 + u_1\nu^2 + O(\nu^4). \tag{4.22}$$

The equality of the leading $u_0$ term in (4.21) and (4.22) simply reexpresses the link between the XY model and the SG QFT alluded to in the introduction. Remarkably the coefficient $u_1$ of the first correction is likewise the same in both cases.

Our first application of these formulae is to the scattering phase shifts. Recall the SG model S-matrix (2.12) with (2.16). Introducing the phase shifts by $S_I(\theta|\nu) = \exp(2i\delta_I(\theta|\nu))$, $I = 0, 1, 2$, and expanding in $\nu$ at fixed $\theta$ yields

$$\delta_I(\theta|\nu) = \delta_I(\theta) + \nu^2\delta_I'(\theta) + O(\nu^4). \tag{4.23}$$

By construction $\delta_I(\theta)$ are the phase shifts of the proposed O(2) S-matrix (3.1). The $O(\nu^2)$ coefficients can be related to the lattice artifacts by the relations (4.22), (4.21). They come out as

$$\delta_0'(\theta) = 0, \qquad \delta_1'(\theta) = \frac{\pi\theta}{6}, \qquad \delta_2'(\theta) = -\frac{\pi\theta}{12}. \tag{4.24}$$

This is used to predict the leading lattice artifacts in the phase shift analysis of Section 5.

It is also feasible to calculate the leading lattice artifacts for the two-point function of the Noether current. In [4] this was done in two-loop perturbation theory. Alternatively, using the current form factors of the SG model, the leading artifacts can also be calculated non-perturbatively via the form factor bootstrap. We worked out the two-particle contribution to this correction. The comparison with numerical data is presented in Section 6.

# 5. MC results for the phase shifts

We begin by numerically investigating the S-matrix. It is the prime input for the boot-strap formulation and an appreciable discrepancy to the bootstrap result (3.1) would immediately rule out that the O(2) bootstrap theory describes the continuum limit of the XY model. The technique to numerically determine the S-matrix takes advantage of the fact that the large volume dependence of the spectrum in a periodic (spatial box) encodes information on the infinite volume S-matrix. For example the volume dependence of the (stable) 1–particle mass is governed by the forward scattering amplitude [32], and a determination of the low-lying two–particle spectrum gives a measurement of the low energy two-particle phase shifts [31]. Here we restrict the discussion to a field theory in $1+1$ dimensions, i.e. the "spatial box" in this case is just a circle of circumference $L$. To our knowledge the first attempt to determine the phase shifts of the XY model was by Vohwinkel [49], and we record his results in Appendix F.

## 5.1 1-particle masses

We chose to measure on the same lattices as Vohwinkel, firstly since they are practical and secondly for having the advantage of being able to compare independent measurements. These lattices are listed in Table 1 together with the measured 1–particle masses. In each case the "time" extent of the lattice is $T = 2L$ and periodic boundary conditions are imposed in each direction.

| $K$ | $L$ | $m(L)$ [49] | $m(L)$ |
|------|-----|-------------|-----------|
| 0.86 | 64 | 0.1711(1) | 0.17096(4) |
| 0.92 | 128 | 0.09465(3) | 0.09461(6) |
| 0.97 | 256 | 0.04620(1) | 0.04603(14) |

Table 1: Values of $K$ and $L$ used in the measurements, with the 1-particle mass $m(L)$ [49] obtained by Vohwinkel [49] and our measurements, $m(L)$.

What is quoted are the results for the single particle masses obtained by fitting the zero-momentum spin 2-point function with a 2-mass formula, with the second mass constrained to be $m_2 = 3m_1$. (The 1-mass fit and the unconstrained 2-mass fit give the same values for $m_1$ within the errors.) The three different values of $K$ correspond to correlation lengths $\sim 6, 11, 22$. In all cases there is good agreement with the results of Vohwinkel.

All the lattices are chosen to have $m(L)L > 10$, so that finite volume effects on the 1–particle masses are expected to be very small according to Eq. (4.6). We denote the resulting 1-particle mass by $m$.

| $K$ | $L$ | $m(L)$ | $D$ | $D_{\text{theor}}$ |
|------|------|-----------|-------------|--------------------|
| 0.86 | 32 | 0.17135(3) | 0.0023(4) | 0.0022 |
| 0.92 | 64 | 0.09478(3) | 0.0018(10) | 0.0012 |
| 0.97 | 128 | 0.04622(4) | 0.0041(39) | 0.0014 |

Table 2: 1–particle masses and finite volume effects.

In order to quantitatively test the latter expectation we measured the 1-particle masses on lattices with the same three bare couplings $K$ as those in Table 1 but with half the previous spatial extent. Our results are listed in Table 2. Also shown are the measured values of the finite volume mass shifts $D = (m(L) - m(2L))/m(2L)$ and $D_{\text{theor}}$ computed from Eq. (4.6). At the smallest correlation length the measured shift is completely consistent with our ansatz for the candidate S-matrix. However, lattice artifacts are to be expected and unfortunately our measurements at the larger correlation lengths are too imprecise to study these effects.

## 5.2 Phase shifts

For a numerical test of the proposed S-matrix (3.1) it is useful not to presuppose the symmetry enhancement. That is we adopt the generic O(2) invariant parameterization (2.12) with $n = 2$. In terms of the $S_I(\theta)$ the phase shifts are defined as

$$S_I(\theta) = \exp\left\{2i\delta_I(\theta)\right\}, \tag{5.1}$$

and can simplified to

$$\delta_0(\theta) = \delta_1(\theta) + \frac{\pi}{2} - \arctan\frac{\theta}{\pi}, \tag{5.2a}$$

$$\delta_1(\theta) = \int_0^\infty \frac{dw}{w} \frac{\sin w\theta}{(1 + e^{\pi w})}, \tag{5.2b}$$

$$\delta_2(\theta) = \delta_1(\theta) - \frac{\pi}{2}. \tag{5.2c}$$

The last relation is responsible for the symmetry enhancement discussed in section 3.1.

To measure the phase shifts on the lattice one sets out to determine the center-of-mass momenta of 2-particle eigenstates of the transfer matrix, since due to the periodic boundary condition in the spatial direction these momenta are quantized according to

$$p_n L + 2\delta(\theta_n) = 2\pi n \,, \qquad p_n = m \sinh \frac{1}{2}\theta_n \,. \tag{5.3}$$

To accomplish this one measures correlators

$$C_{xy}^{(I)}(t) = \langle O_I(x,0) O_I(y,t) \rangle \,, \tag{5.4}$$

where the $O^{(I)}$ are 2-spin operators with zero total momentum in the isospin channels $I = 0, 1, 2$:

$$O_I(x,t) = \frac{1}{L} \sum_{z=0}^{L-1} (P_I)_{1b_I}^{cd} \, S^c(z,t) S^d(z+x,t) \,, \quad b_0 = 1 \,, b_1 = b_2 = 2 \,, \tag{5.5}$$

the $P_I$ being the projectors in Eq. (2.14). Taking $T$ large enough so that terms proportional to $\mathrm{e}^{-2mT}$ can be neglected, one has

$$C_{xy}^{(I)}(t) = \sum_n \mathrm{e}^{-E_n t} \psi_n^{(I)}(x) \psi_n^{(I)}(y) \,, \tag{5.6}$$

where

$$\psi_n^{(I)}(x) = \langle \mathrm{vac}| O_I(x,0) |n \rangle \,, \tag{5.7}$$

is the "wave function" of the corresponding state. In the $I = 0$ channel the vacuum also contributes as an intermediate state. In this case one can subtract this contribution from the beginning, i.e. consider the connected correlator. Alternatively, one can take the full $I = 0$ correlator, keeping in mind that in this case the vacuum is the lowest energy intermediate state.

Now there are at least two ways to proceed. The first is to extract the energies $E_n$ of the 2-particle states which dominate the correlation function Eq. (5.6) for sufficiently large $t$, and then compute the corresponding center of mass momenta via

$$E_n = 2E^{(1)}(p_n) = 2\sqrt{p_n^2 + m^2} \,. \tag{5.8}$$

This was the strategy used in the pioneering paper of Lüscher and Wolff [31] and adopted by Vohwinkel in his studies [49]. In Eq. (5.8) lattice artifacts have been neglected and the physical volume is taken so large that the finite volume dependence of the single particle masses is negligible.

In ref. [6] an alternative was suggested which starts from the observation that the relative momentum $2p_n$ of the two particles is also encoded in the wave function: in the symmetric channels $(I = 0, 2)$ one should have

$$\psi_n(x) = A \cos p_n(x - L/2), \text{ for } R < x < L - R, \tag{5.9}$$

and similarly with $\sin p_n(x - L/2)$ for the $I = 1$ channel. Here $R$ is the "interaction range" characterized by the requirement that for a relative distance $x > R$ the two particles propagate essentially freely. Note that Eq. (5.3) assumes that the box is large enough to accommodate the two particles without "squeezing" them, i.e. $L/2 > R$.

The rank $N$ of the matrix $C(t)$ in Eq. (5.6) is $L/2$, $L/2 - 1$ and $L/2 + 1$ in the $I = 0, 1, 2$ channels, respectively. (This is when the connected correlation function is considered in the $I = 0$ channel, otherwise $N = L/2 + 1$ also in this channel.) We assume that for $t \geq t_0$ (with some $t_0$) no more than $N$ states contribute to $C_{xy}^{(I)}(t)$, i.e. that the contribution from the states $n > N$ can be neglected completely.

Lüscher and Wolff [31] suggested to determine the energies $E_n$ from the generalized eigen-value problem[*]

$$C(t)v_n = \lambda_n(t, t_0)C(t_0)v_n . \tag{5.10}$$

Provided the sum in Eq. (5.6) is restricted to $N$ terms, $1 \leq n \leq N$, the eigenvalues of Eq. (5.10) are given *exactly* by

$$\lambda_n(t, t_0) = e^{-E_n(t-t_0)} . \tag{5.11}$$

It is easy to show that (apart from the normalization)

$$\psi_n(x) = \sum_y C_{xy}(t_0)v_n(y) . \tag{5.12}$$

A problematic feature of the generalized eigenvalue equation (5.10) is that its solutions become unstable if $C(t_0)$ has very small eigenvalues. This can be seen by observing that $\lambda_n(t, t_0)$ are the eigenvalues of the ordinary eigenvalue equation for the matrix $C(t_0)^{-1/2}C(t)C(t_0)^{-1/2}$. Of course, the exact correlation matrix $C(t_0)$ is positive definite, but the statistical noise will spoil this property, and the measured matrix can have even negative eigenvalues, especially for larger values of $t_0$ and for large number of operators $N$. For this reason in ref. [31] $N \sim L/4$ operators were used (actually, in momentum space rather then in $x$-space) and the values of $t_0$ were restricted to 0 and 1.

___

[*]This equation was considered already earlier by Michael [35], in connection with a variational approach evaluating the static potential in lattice gauge theory.

To avoid the instability, we restrict first the correlation matrix to an $M$-dimensional sub-space ($M < N$) spanned by the first $M$ eigenvectors of $C(t_0)$ with the largest eigenvalues (still stable against the statistical fluctuations) [6, 37]. The generalized eigenvalue problem is then written for the new correlation matrix $\overline{C}(t)$ in this reduced basis. Of course, to read off the momenta, the wave functions have to be transformed back into the original basis labeled by the relative distance $x$.

Following refs. [35, 31] one can obtain $E_n$ from the plateau of the "effective energy"

$$E_n^{\text{eff}}(t) = \ln \frac{\lambda_n(t, t_0)}{\lambda_n(t+1, t_0)} \,, \tag{5.13}$$

and determine the corresponding momentum $p_n$ from Eq. (5.8).

The alternative way is to fit the wave function $\psi_n(x)$ by the ansatz in Eq. (5.9) for $x_0 \leq x \leq L/2$. We have verified that it is safe to take $x_0 \geq 3/m$. There is also a large window where the results are not sensitive to the variation of $M$, for different choices of $t_0$. For the largest correlation length $\xi_{\text{exp}} \approx 21.6$ we could take $t_0$ as large as 10, which would be impossible without the preceding truncation.

In [6] we concluded that the wave function method has somewhat smaller errors and is more stable. In particular the smallest momentum obtained from the 2-particle energy is quite sensitive to the error in the single particle mass, while in the wave function method the value of this mass is not used at all. Although we measured the phase shifts by both methods and checked their consistency, only our results from the wave function method will be presented here. Vohwinkel's results on the energy levels are recorded in Table 15.

Fig. 1 shows the wave functions of the first six 2-particle states in the $I = 0$ channel obtained using Eqs. (5.10), (5.12). Fig. 2 displays the deviations of the first three wave functions from the corresponding free one, $A \cos p(x - L/2)$ in the $I = 0$ channel. As expected, the true wave functions deviate from the free ones only for small relative distances of O($\xi_{\text{exp}}$). The plots illustrate that the momentum $p$ can be determined quite precisely by fitting the wave function in some properly chosen range $x_0 \leq x \leq L/2$. Note, however, that in Eq. (5.3) the momentum $p_n$ is multiplied by $L$, hence it has to be determined to good precision in order to yield a reasonable error for the phase shift. In our simulations therefore only the phase shifts at the first 3–4 momenta could be determined with a reasonable error.
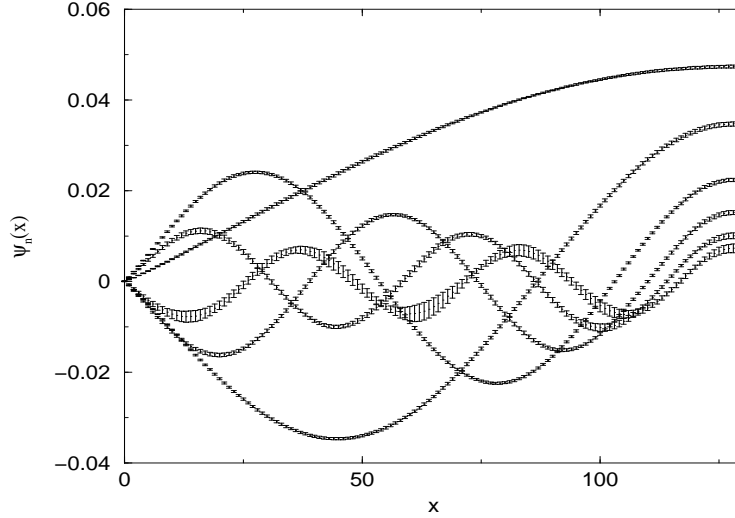
Figure 1: The first six wave functions $\langle \text{vac}|O_I(x)|n\rangle$ in the $I = 0$ channel for $K = 0.97$, $L = 256$.
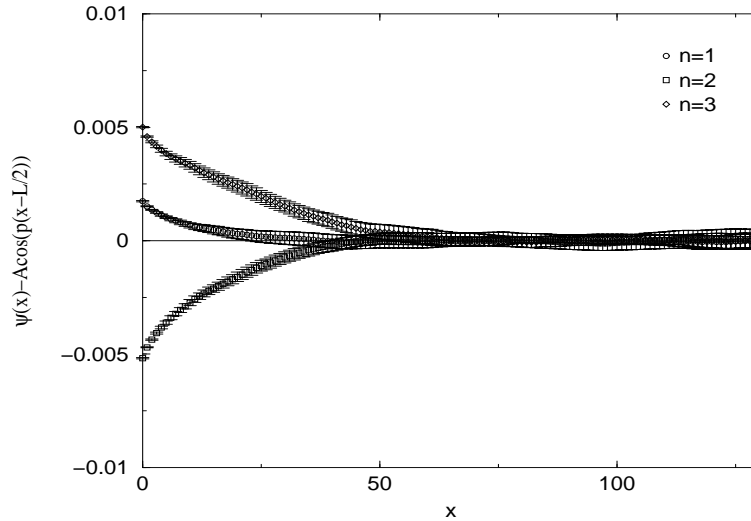


Figure 2: Deviations of the first 3 wave functions from the ansatz $A\cos p(x - L/2)$.

A summary of our measurements of the phase shifts is given in Table 3. The Figures 3 to 5 compare these results with the theoretical curves of Eqs. (5.2a-c). The leading lattice artifacts according to Eq. (4.24) for the largest correlation length $\xi_{\text{exp}} = 21.645(5)$ are also shown. The present overall results are certainly consistent with the theoretical expectations.

| $K$ | $L$ | $I$ | $n$ | $p/m$ | $[p/m]_{\mathrm{ex}}$ | $\delta^{(I)}(p)$ | $[\delta^{(I)}(p)]_{\mathrm{ex}}$ |
|---|---|---|---|---|---|---|---|
| 0.86 | 64 | 0 | 1 | 0.297(3) | 0.2976 | 1.517(15) | 1.5138 |
| | | | 2 | 0.885(2) | 0.8895 | 1.446(12) | 1.4186 |
| | | | 3 | 1.468(4) | 1.4760 | 1.397(20) | 1.3529 |
| 0.92 | 128 | 0 | 1 | 0.269(1) | 0.2677 | 1.512(8) | 1.5193 |
| | | | 2 | 0.804(1) | 0.8007 | 1.413(6) | 1.4307 |
| | | | 3 | 1.330(2) | 1.3297 | 1.366(11) | 1.3669 |
| 0.97 | 256 | 0 | 1 | 0.272(7) | 0.2745 | 1.535(43) | 1.5180 |
| | | | 2 | 0.825(5) | 0.8210 | 1.408(27) | 1.4279 |
| | | | 3 | 1.367(8) | 1.3632 | 1.342(47) | 1.3180 |
| 0.86 | 64 | 1 | 1 | 0.548(6) | 0.5349 | 0.146(34) | 0.2161 |
| | | | 2 | 1.108(3) | 1.0828 | 0.223(16) | 0.3616 |
| | | | 3 | 1.684(4) | 1.6416 | 0.218(19) | 0.4474 |
| 0.92 | 128 | 1 | 1 | 0.495(2) | 0.4855 | 0.140(15) | 0.1992 |
| | | | 2 | 0.999(1) | 0.9806 | 0.231(7) | 0.3405 |
| | | | 3 | 1.511(1) | 1.4846 | 0.265(7) | 0.4280 |
| 0.97 | 256 | 1 | 1 | 0.491(16) | 0.4969 | 0.237(94) | 0.2031 |
| | | | 2 | 1.024(7) | 1.0041 | 0.230(42) | 0.3455 |
| | | | 3 | 1.535(6) | 1.5205 | 0.350(36) | 0.4328 |
| 0.86 | 64 | 2 | 1 | 0.260(2) | 0.2663 | $-1.423(11)$ | $-1.4562$ |
| | | | 2 | 0.790(1) | 0.8072 | $-1.179(6)$ | $-1.2726$ |
| | | | 3 | 1.334(2) | 1.3612 | $-1.014(10)$ | $-1.1607$ |
| 0.92 | 128 | 2 | 1 | 0.236(1) | 0.2419 | $-1.433(7)$ | $-1.4660$ |
| | | | 2 | 0.721(1) | 0.7318 | $-1.228(5)$ | $-1.2930$ |
| | | | 3 | 1.213(1) | 1.2317 | $-1.067(7)$ | $-1.1812$ |
| 0.97 | 256 | 2 | 1 | 0.242(6) | 0.2475 | $-1.432(38)$ | $-1.4638$ |
| | | | 2 | 0.739(4) | 0.7491 | $-1.230(21)$ | $-1.2881$ |
| | | | 3 | 1.262(7) | 1.2614 | $-1.181(41)$ | $-1.1763$ |

Table 3: The phase shifts $\delta_I(p)$ for the first 3 states ($n = 1, 2, 3$) in different isospin channels, with the values of $p/m$ determined from the wave function. The continuum results $[p/m]_{\mathrm{ex}}$ and $[\delta_I(p)]_{\mathrm{ex}}$ calculated from the S-matrix are also given.
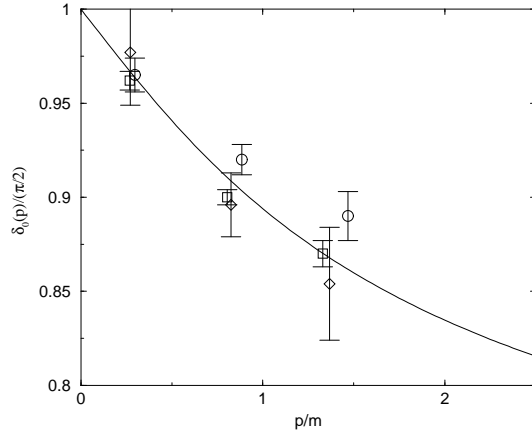
Figure 3: $I = 0$ phase shifts. Points denoted by circle, square and diamond correspond to correlation length $\approx$ 6, 11 and 22, respectively. The solid line is the continuum result, Eq. (5.2a).
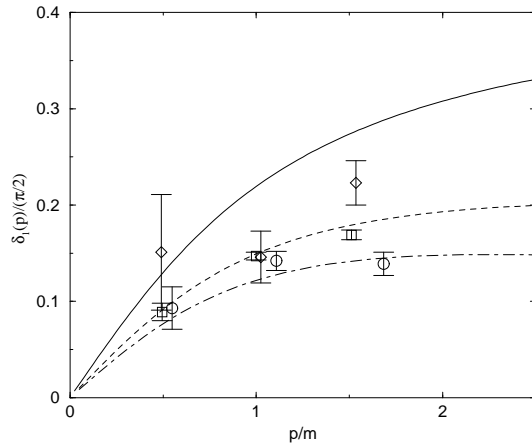


Figure 4: $I = 1$ phase shifts. The notations for data points are the same as in Fig. 3. The solid line is the continuum result, the other two lines include leading corrections due to finite $\xi_{\exp}$ of Eq. (4.24) with $u = 1.46$ (see [21]): the dashed line for $\xi_{\exp} \approx 22$, the dot-dashed line for $\xi_{\exp} \approx 11$.
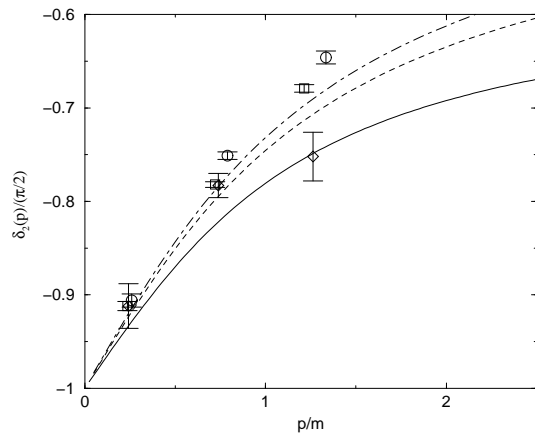
Figure 5: $I = 2$ phase shifts. The notations are the same as in Fig. 4.

# 6. MC results for correlation functions and 4-point coupling

Here we describe our MC results for the intrinsic 4-point coupling $g_R$ and for the current and spin 2-point correlation functions in Fourier space. In addition we reconsider some aspects of the Kosterlitz-Thouless (KT) theory.

A list of the lattices considered together with some of the MC results is given in Table 4. We group the lattices into families labeled 1 to 12. Members of a given family correspond to the same coupling $K$ but different size $L$. Throughout this section $\xi$ denotes the second moment correlation length (4.9), which is a function of $K$ and $L$. We denote the 'apparent' physical size of the lattice by $z' = L/\xi(K, L)$. For most lattices we made 200k measurements where we measured all the physical quantities above supplemented by an additional 2M measurements for the "bulk" quantities ($\xi$, $\chi$ and $g_R$) only. We also took data on 'thermodynamic' lattices ($L/\xi \approx 14$). These are reported in Appendix E. We did not use them in our analysis because there were some not completely understood inconsistencies between data taken on different machines, with different random number generators and different programs.

## 6.1 KT theory

We begin by studying the dependence of the correlation length $\xi$ and the susceptibility $\chi$ on the coupling $K$ and compare our MC results to the predictions of the KT theory. For this purpose we first need to extrapolate the measured values of $\xi$ and $\chi$ to infinite volume. This is done by a finite size scaling analysis.

For fixed coupling the size dependence of the correlation length is assumed to be given by

$$\ln \xi(K, L) = \ln \xi(K, \infty) + z^{A_2} e^{-z} \left[ C_0^\xi(K) + C_1^\xi(K) \frac{1}{z} + \ldots \right]. \qquad (6.1)$$

Here $z := L/\xi_{\exp}(K, \infty)$ where $\xi_{\exp}$ is the true ("exponential") correlation length. $\xi_{\exp}$ is expected to be very close to the second moment correlation length: the form factor bootstrap predicts $\xi_{\exp}/\xi = \sqrt{\gamma_2/\delta_2} = 1.00089$ and the lattice models are certainly not very far from the form factor construction; therefore at our $\approx 0.001$ accuracy the distinction between the two correlation lengths can be neglected. For the exponent in (6.1) we expect $A^\xi = A_2 = -1/2$ on account of the considerations outlined in Section 4.3, but we also tried different values of that exponent in order to see if the data indeed support this expectation.

| label | $K$ | $L$ | $\xi$ | $\chi$ | $g_{\mathrm{R}}$ | $z'$ |
|---|---|---|---|---|---|---|
| 1 | 0.86 | 24 | 5.728(1) | 57.07(11) | 7.533(3) | 4.2 |
| 1 | 0.86 | 29 | 5.795(1) | 58.82(12) | 8.147(4) | 5.0 |
| 1 | 0.86 | 32 | 5.815(2) | 59.33(2) | 8.357(8) | 5.5 |
| 1 | 0.86 | 40 | 5.833(1) | 59.814(9) | 8.672(7) | 6.9 |
| 1 | 0.86 | 64 | 5.839(1) | 59.956(7) | 8.774(14) | 11.0 |
| 2 | 0.92 | 42 | 10.314(2) | 153.76(4) | 7.484(3) | 4.1 |
| 2 | 0.92 | 52 | 10.466(2) | 159.58(4) | 8.201(5) | 5.0 |
| 2 | 0.92 | 68 | 10.536(2) | 162.28(4) | 8.690(8) | 6.5 |
| 2 | 0.92 | 94 | 10.548(5) | 162.79(7) | 8.855(27) | 8.9 |
| 3 | 0.93 | 64 | 11.861(4) | 198.05(7) | 8.436(10) | 5.4 |
| 3 | 0.93 | 80 | 11.905(2) | 199.95(3) | 8.755(7) | 6.7 |
| 4 | 0.97 | 86 | 21.146(4) | 525.11(11) | 7.539(2) | 4.1 |
| 4 | 0.97 | 108 | 21.467(6) | 545.85(17) | 8.313(6) | 5.0 |
| 4 | 0.97 | 136 | 21.589(9) | 553.88(28) | 8.745(21) | 6.3 |
| 4 | 0.97 | 194 | 21.633(11) | 556.33(29) | 8.934(26) | 9.0 |
| 5 | 0.975 | 128 | 23.546(6) | 641.53(19) | 8.514(9) | 5.4 |
| 6 | 1.00 | 160 | 39.219(8) | 1522.2(4) | 7.585(3) | 4.1 |
| 6 | 1.00 | 200 | 39.801(7) | 1581.2(4) | 8.345(4) | 5.0 |
| 6 | 1.00 | 256 | 40.025(11) | 1605.0(5) | 8.798(10) | 6.4 |
| 6 | 1.00 | 360 | 40.104(15) | 1611.2(7) | 8.955(22) | 9.0 |
| 7 | 1.005 | 256 | 45.247(13) | 1980.7(6) | 8.618(9) | 5.7 |
| 8 | 1.0174 | 360 | 63.889(22) | 3596.4(1.2) | 8.631(10) | 5.6 |
| 8 | 1.0174 | 500 | 64.314(91) | 3639.2(6.2) | 9.05(12) | 7.8 |
| 9 | 1.02 | 276 | 67.934(45) | 3936.7(3.1) | 7.587(7) | 4.1 |
| 9 | 1.02 | 344 | 68.942(47) | 4091.1(3.0) | 8.375(13) | 5.0 |
| 9 | 1.02 | 560 | 69.500(25) | 4170.6(1.8) | 8.997(18) | 8.1 |
| 10 | 1.04 | 578 | 142.09(15) | 14164.(20.) | 7.600(15) | 4.1 |
| 10 | 1.04 | 726 | 144.43(12) | 14743.(15.) | 8.404(18) | 5.0 |
| 11 | 1.05 | 930 | 230.10(29) | 32589.(46.) | 7.586(19) | 4.0 |
| 11 | 1.05 | 1160 | 232.83(22) | 33800.(37.) | 8.392(19) | 5.0 |
| 12 | 1.06 | 2100 | 418.0(1.6) | 93724.(428.) | 8.410(79) | 5.0 |

Table 4: Lattice parameters and results.

We produce a global fit of the finite size effects by fitting all the data in Table 4 to the form (6.1) truncating after the $C_0^\xi$ term and taking $C_0^\xi$ to be independent of $K$. The values of $\xi(K,\infty)$ are fit parameters, one for each of the twelve families. Since initially we do not know the values of $L/\xi(K,\infty)$ we first replace it by $L/\xi(K,L)$; this leads to a first estimate of $\xi(K,\infty)$ which is then used in the fit ansatz. Iterating this procedure about 5 times leads to convergence of our extrapolated values of $\xi(K,\infty)$. It turns out that this type of fit favors a value of $A_2$ near $-1/2$ in agreement with expectation; for this value of the exponent we obtain $\text{chi}^2/\text{dof} = 0.9$ with 19 degrees of freedom.

Furthermore, including a $C_1^\xi$ term makes the fit very insensitive to the value of the exponent $A_2$, both as far as the fit quality and the extrapolated values of $\xi(K,\infty)$ are concerned. For $A_2 = -1/2$ the coefficient $C_1^\xi$ comes out consistent with zero. Therefore in Table 5 we only report the values obtained with the simplest fit with $A_2 = -1/2$ and only one finite size correction term.

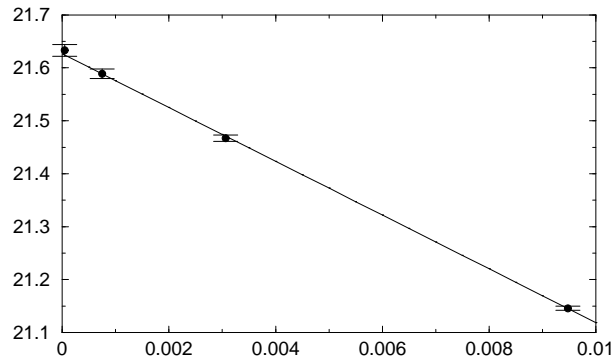Figure 6 illustrates the $z$ dependence of the correlation length for $K = 0.97$.



Figure 6: $\xi(K,L)$ vs. $\exp(-z)/\sqrt{z}$ at $K = 0.97$.

The FS analysis of the susceptibility is analogous, but we don't need any iteration, since we start already with the right $z$ values. Again the data favor a value near $-1/2$ if we truncate with the $C_0^\chi$ term, and if we include the next term, the fit becomes insensitive to $A_2$. In Table 5 we present the results from the simplest fit assuming $A_2 = -1/2$, which has a $\text{chi}^2/\text{dof}$ of 0.7 with 19 degrees of freedom.

Next we study the $K$-dependence of the infinite volume quantities. One of the best known predictions of KT theory [28] is the unusual coupling dependence of the correlation length. Close to the critical point $K_c$, $\xi$ is predicted to diverge as $\xi \sim \exp(b/\sqrt{\tau})$, where $\tau = K_c - K$ is the reduced coupling and $b$ is a non-universal constant. In more detail, the Sine-Gordon description of the KT transition entails (using eqs. (8.13) and (8.14) of

[1] *)

$$\ln \xi(K, \infty) = \frac{b}{\sqrt{\tau}} - u + c\sqrt{\tau} + \dots, \tag{6.2}$$

where $u$ and $c$ are again non-universal constants and the dots stand for higher powers in $\tau$. We fitted the $\xi(K, \infty)$ data to the form (6.2) without higher terms, leaving out different numbers $n_{\mathrm{skip}}$ of the low $\xi$ families to see how stable the fit parameters are. The results are presented in Table 6. Note that some of the fits have an unacceptable chi$^2$. In any case, the determination of $u$ is not very stable. This situation could be a sign of the inappropriateness of the ansatz (6.2), or of some problem with our data or it could mean that we are still too far from the critical point, so that asymptotic formulae cannot yet be applied reliably. In further fits below that do involve $u$, we use the value appropriate to the number of discarded families. A visual illustration of the $n_{\mathrm{skip}} = 1$ fit is shown in the left part of Fig. 7.

We should mention that Hasenbusch and Pinn [21] have determined the constants $b$ and $u$ by their method of matching to the exactly solvable BCSOS model; their values are $u = 1.46(1)$ and $b = 1.879(4)$, in rough agreement at least with some of our estimates. It should be noted, however, that their method avoids the problem of controlling subleading corrections like the third term in eq. (6.2).

| $K$ | 0.86 | 0.92 | 0.93 | 0.97 | 0.975 | 1.00 |
|---|---|---|---|---|---|---|
| $\xi(K, \infty)$ | 5.8391(5) | 10.549(1) | 11.918(2) | 21.627(4) | 23.655(6) | 40.096(5) |
| $\chi(K, \infty)$ | 59.962(5) | 162.86(26) | 200.52(28) | 556.32(11) | 649.15(19) | 1611.4(3) |

| $K$ | 1.005 | 1.0174 | 1.02 | 1.04 | 1.05 | 1.06 |
|---|---|---|---|---|---|---|
| $\xi(K, \infty)$ | 45.410(13) | 64.137(22) | 69.505(20) | 145.424(95) | 234.93(18) | 421.1(1.6) |
| $\chi(K, \infty)$ | 1999.1(6) | 3631.1(1.2) | 4173.0(1.4) | 15017.(13.) | 34512.(30.) | 95502.(436.) |

Table 5: Correlation length and susceptibility extrapolated to infinite volume using a global fit.

KT theory also predicts the asymptotics of $\chi(\xi)$ for large $\xi$ (at least up to possible logarithmic corrections),

$$\chi \sim \xi^{2-\eta}, \quad \text{with} \quad \eta = 1/4. \tag{6.3}$$

A linear fit of $\ln \chi$ versus $\ln \xi$ is shown in Fig. 7. The slope is 1.73, which is very close to the expected result. The fit is visually good, but even if we omit families 1,2 and 3 we get a huge value of chi$^2$/dof $\approx 288/7$, indicating the presence of non-negligible subleading terms. Irving and Kenna [25], following Butera and Comi [11] (see also [22]) argued that

---

*note that (8.15) contains a misprint.

| $n_{\text{skip}}$ | $b$ | $u$ | chi$^2$/dof |
|---|---|---|---|
| 1 | 1.865(1) | 1.280(8) | 27/8 |
| 2 | 1.866(2) | 1.286(9) | 27/7 |
| 3 | 1.875(3) | 1.340(16) | 11/6 |
| 4 | 1.873(4) | 1.332(21) | 11/5 |
| 5 | 1.886(1) | 1.414(40) | 4.9/4 |
| 6 | 1.885(9) | 1.406(58) | 4.9/3 |
| 7 | 1.86(2) | 1.22(15) | 3.3/2 |
| 8 | 1.86(3) | 1.21(18) | 2.2/1 |

Table 6: Fit of the infinite volume correlation length to the ansatz (6.2); $n_{\text{skip}}$ denotes the number of low $\xi$ families discarded.
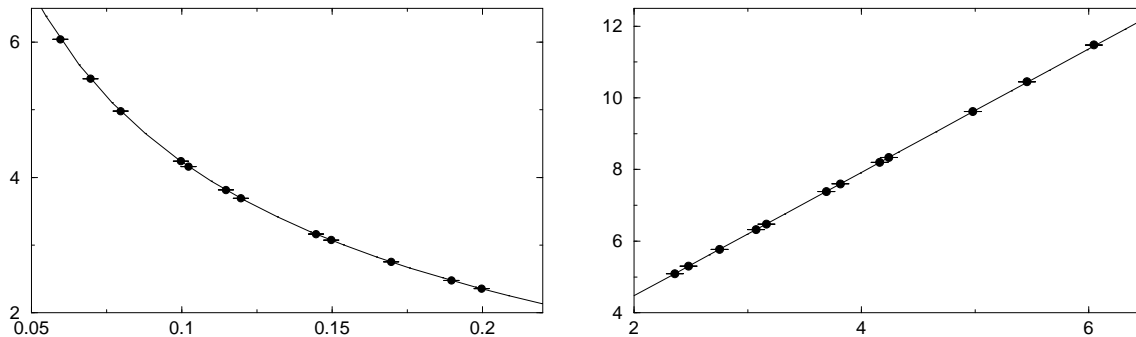


Figure 7: Illustration of KT scenario: Left, $\ln \xi$ versus $\tau$ and a fit to (6.2). Right, $\ln \chi$ versus $\ln \xi$ and a linear fit.

the Kosterlitz-Thouless theory implies the following refinement of (6.3):

$$\chi \sim \xi^{2-\eta}(\ln \xi)^{-2r}\,, \tag{6.4}$$

with $r = -1/16$. This would in particular mean that $\chi$ grows faster than $\xi^{1.75}$, whereas the data on the contrary indicate a slower increase.

On the other hand one of us [4] has argued that the Kosterlitz-Thouless theory implies $r = 0$, with a specific additive correction to (6.3): the renormalization group invariant quantity $Q$ was introduced, which for large $\xi$ behaves as

$$Q = \frac{\pi^2}{2(\ln \xi + u)^2} + O\left\{(\ln \xi)^{-5}\right\}\,. \tag{6.5}$$

38

It was then argued that the correct asymptotic formula, instead of (6.4), is

$$\ln \chi \sim \frac{7}{4} \ln \xi + O(Q). \tag{6.6}$$

Taking $u$ from Table 6 the relation (6.6) can again be tested against the data. We fitted $\ln \chi - 1.75 \ln \xi$ against $Q$, discarding successively more and more low $\xi$ families; in the fits we used the best value of $u$ corresponding to the same number of discarded families. The results are given in Table 7.

| $n_{\mathrm{skip}}$ | 1 | 2 | 3 | 4 | 5 | 6 | 7 | 8 |
|---|---|---|---|---|---|---|---|---|
| chi$^2$/dof | 44/9 | 32/8 | 8.2/7 | 5.4/6 | 2.9/5 | 0.6/4 | 0.5/3 | 0.5/2 |

Table 7:  Fits of $\ln \chi - 1.75 \ln \xi$ to linear function of $Q$; $n_{\mathrm{skip}}$ denotes the number of low $\xi$ families discarded.

Starting with $n_{\mathrm{skip}} = 3$ the fits are acceptable, but of course it should be remembered that we are not quite sure which value of $u$ should be used. We do not list the fit parameters, but they are quite stable. So one can say the data support the prediction (6.6).
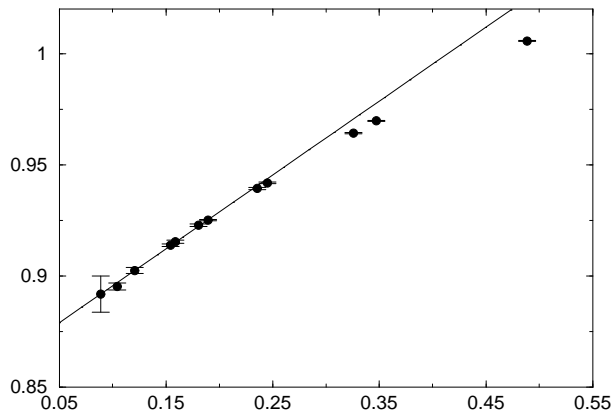


Figure 8:  $\ln \chi - 1.75 \ln \xi$ versus $Q$ and a linear fit on the data from the $\xi \geq 39$ lattices.

We will use the variable $Q$ as the quantity characterizing the distance from the continuum limit.

## 6.2 Determination of $g_{\mathrm{R}}$

Lattice determinations of $g_{\mathrm{R}}$ can be based either on the high temperature expansion or on numerical simulations. The results obtained via the high temperature expansion and

the standard action (4.1) are

$$g_R = 9.15(10) \ [10] \qquad g_R = 9.10(5) \ [40].$$ (6.7)

In the numerical simulations we again aimed at achieving a precision of better than one percent. For the necessary extrapolation to the infinite volume we use the procedure outlined before, i.e. we fit the data to the ansatz

$$\ln g_R(K, L) = \ln g_R(K, \infty) + z^{A_4} e^{-z} \left[ C_0^{g_R}(K) + C_1^{g_R}(K) \frac{1}{z} + \dots \right],$$ (6.8)

where, as described in Section 4.3, there are arguments suggesting $A^{g_R} = A_4 = 1/2$. As opposed to the situation with $\xi$ and $\chi$, with this value, the leading finite size correction alone does not properly describe the FS dependence. If we instead use the optimized value $A_4 = 0.8$, a subleading finite size correction is not needed. It is gratifying that the extrapolated values are almost independent of which of the two options we choose. We report the infinite volume values obtained with $A_4 = 1/2$ and two FS correction terms as well as those with only the leading FS correction and $A_4 = 0.8$ in Table 8. Both fits have a chi$^2$/dof around 1.

| $K$ | 0.86 | 0.92 | 0.93 | 0.97 | 0.975 | 1.00 |
|---|---|---|---|---|---|---|
| $g_R(K, \infty)$ | 8.790(6) | 8.877(6) | 8.900(7) | 8.952(6) | 8.967(11) | 8.989(6) |
| $g_R(K, \infty)$ | 8.794(3) | 8.882(4) | 8.906(6) | 8.958(4) | 8.973(10) | 8.995(4) |

| $K$ | 1.005 | 1.0174 | 1.02 | 1.04 | 1.05 | 1.06 |
|---|---|---|---|---|---|---|
| $g_R(K, \infty)$ | 8.993(10) | 9.015(11) | 9.026(8) | 9.039(14) | 9.053(16) | 9.062(9) |
| $g_R(K, \infty)$ | 8.999(9) | 9.022(10) | 9.031(7) | 9.044(13) | 9.058(15) | 9.067(9) |

Table 8: Fits to $g_R$ with $A_4 = 1/2$ using 2 finite size parameters (upper line) and with $A_4 = 0.8$ using only the leading finite size parameter (lower line).

Finally we turn to the continuum limit of $g_R$. One of us [4] has argued that the leading lattice artifacts are proportional to the quantity $Q$, which in turn depends on the parameter $u$ extracted from the fits in table 6. We present in Table 9 the results of fits of the infinite volume $g_R$ values to a linear function of $Q$; we are reporting the results obtained by discarding different numbers of low $\xi$ values, obtained with the corresponding $u$ value. The fits are generally of good quality, but the resulting continuum values of $g_R$ depend noticeably on the number of skipped values.

Our MC results are to be compared with the result of the form factor computation from Appendix D

$$g_R = 9.10(4).$$ (6.9)

| $n_{\text{skip}}$ | $g_{\text{R}}(K_c, \infty)$ | chi$^2$/dof | $g_{\text{R}}(K_c, \infty)$ | chi$^2$/dof |
|---|---|---|---|---|
| 1 | 9.124(8) | 2.2/9 | 9.129(7) | 4.4/9 |
| 2 | 9.120(10) | 2.4/8 | 9.124(9) | 3.5/8 |
| 3 | 9.127(15) | 2.1/7 | 9.132(12) | 3.0/7 |
| 4 | 9.125(20) | 2.1/6 | 9.131(18) | 3.0/6 |
| 5 | 9.140(25) | 1.4/5 | 9.148(22) | 1.6/5 |
| 6 | 9.134(33) | 1.3/4 | 9.138(31) | 1.4/4 |
| 7 | 9.108(40) | 0.4/3 | 9.112(38) | 0.3/3 |
| 8 | 9.099(43) | 0.8/2 | 9.105(41) | 0.9/2 |

Table 9: Fits of $g_{\text{R}}(K, \infty)$ to a linear function of $Q$; $n_{\text{skip}}$ denotes the number of low $\xi$ families discarded. The two columns correspond to the two rows of Table 8.

## 6.3 The current correlation function

Here we compare the bootstrap result for the current two-point function (2.11) with the lattice measurements. The extrapolation of the lattice data to the continuum is done by means of a two-step procedure, which is a variant of the method used for $g_{\text{R}}$. We first perform a FS analysis for those relatively short correlation lengths for which we could afford to measure the correlation function on lattices of large physical size. Using the FS scaling coefficients determined this way we are able to extrapolate the results of our measurements, corresponding to moderately large physical size, to infinite size. In the second step we take the continuum limit by extrapolating our results for infinite correlation length.

For the first step we adopt an additive form of the FS scaling hypothesis:

$$I(q; K, L) = I(q; K, \infty) + z^{A^I} e^{-z} \left[ C_0^I(q; K) + C_1^I(q; K) \frac{1}{z} + \cdots \right]. \qquad (6.10)$$

We note that for the WARD case the subtracted correlation function is a linear combination of a 2-point function and a 4-point function; therefore by the arguments used before one expects $A^I = A_4 = 1/2$.

Compared to the case of $g_{\text{R}}$, the analysis here is complicated by momentum dependence and also the fact that we have used two alternative definitions (SUB and WARD) of the current correlation function. To be able to compare the results with each other and with the bootstrap calculation we used the dimensionless momentum variable $q := p/M_R$, where $M_R$ is the second moment mass. We interpolated our lattice results to integer $q$

values $q = 1, 2, \ldots, 50$ by fitting the measured values with the 8-parameter formula

$$I(q) = \sum_{k=3}^{10} m_k \frac{q^2}{k^2 + q^2}. \tag{6.11}$$

This formula is motivated by the spectral representation and with the 8 parameters $\{m_k\}$ it gives excellent representation of the current correlation function for all our lattices in the range $q < 50$.

We fitted the leading coefficient $C_0^I(q)$ (ignoring its $K$ dependence and any subleading terms) using the four data points of families 2, 4 and 6 for the SUB case and families 2 and 4 for the WARD case. (Unfortunately the WARD data are not available for family 6, except for the lattice 6 with $L = 200$.) The results of these fits for $q = 25$ are shown in Figure 9. The fact that the linear fits are nearly parallel shows that our assumption of FS scaling works here. More importantly one sees that the difference between the two definitions disappears at large $z$, as it should[†]. We also note that FS corrections have opposite signs for the SUB and WARD cases and that the latter are much smaller. These qualitative features remain valid also for other $q$-values, although for small momenta the FS corrections for WARD data are no longer minute compared to the SUB ones at the same $q$. On the other hand for larger momenta the difference is even more pronounced.
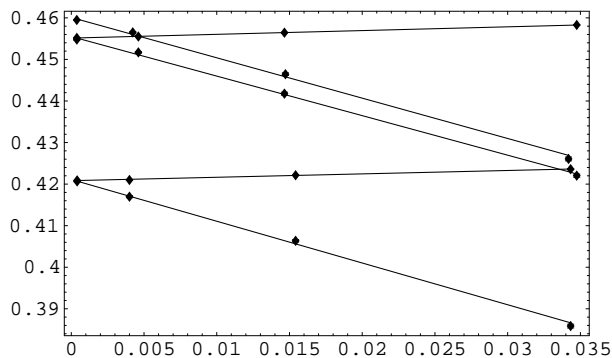


Figure 9: Test of FS scaling: $I(25)$ in SUB and WARD definition versus $\sqrt{z}e^{-z}$. The three (approximately) parallel lines with negative slope correspond to the SUB data; increasing values correspond to families 2, 4 and 6 respectively. The two (approximately) parallel lines with positive slope are the WARD data for families 2 and 4. There are no WARD data available for family 6.

Before turning to the infinite volume extrapolation let us briefly digress on the relative size of the statistical errors in the WARD and SUB data. In Figure 10 these errors are

---

[†]Note that in this analysis we replaced $z$ by $z'$.

shown as a function of the momentum $q$ for both methods, for lattice 12. One sees that, with the exception of the first few points, the WARD data have much smaller statistical errors, for large momenta by about an order of magnitude! This remains true for all other lattices. The explanation is that before subtraction, the zero momentum component of the Fourier transform of the current correlation function has the largest fluctuation and its fluctuations decrease with momentum. Already at $q \sim$ 4-5 the fluctuations are much smaller. If we subtract the zero momentum component, all the SUB points inherit its large error and beyond $q > 5$ the errors are practically constant. On the other hand, since the action density is known with a very good precision the errors of the WARD data points are almost the same as the unsubtracted ones and rapidly decrease with increasing momentum. For $q$ less than $3 \sim 4$, the SUB data have smaller errors since the fluctuations of $I(q)$ and $I(0)$ cancel due to their strong correlation. Because of these two advantages of the WARD method (for not too low momenta), from now on we will use the WARD data exclusively.
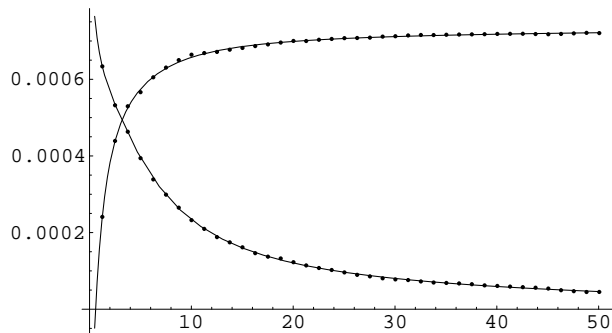


Figure 10: Absolute statistical errors for SUB (increasing) and WARD (decreasing) current data as a function of $q$, for $\xi = 421$, $L = 2100$. The continuous lines are fitted for convenience.

Let us now address the extrapolation to infinite lattice size. This is done by determining the FS coefficients in (6.10) from a small reference lattice and then use them to do the extrapolation for all other lattices. We used lattice family 4 to determine the coefficients, which is the family with four sizes and the largest coupling. Using family 2 instead leads to slightly different results that allow one to estimate the systematic error in the extrapolation procedure. For illustration let us quote the (absolute) statistical error stat($q$) and the (absolute) systematic error sys($q$) obtained thereby at $q = 5, 15, 25$: stat(5) = 0.0002, sys(5) = 0.0006, stat(15) = 0.0001, sys(15) = 0.0003, stat(25) = 0.0001, sys(25) = 0.0001. One sees that the errors are small and the infinite volume extrapolation is under control.

In the final step the extrapolation to infinite correlation length has to be performed. Since the largest lattice 12 already corresponds to a correlation length of $\xi = 418$ one
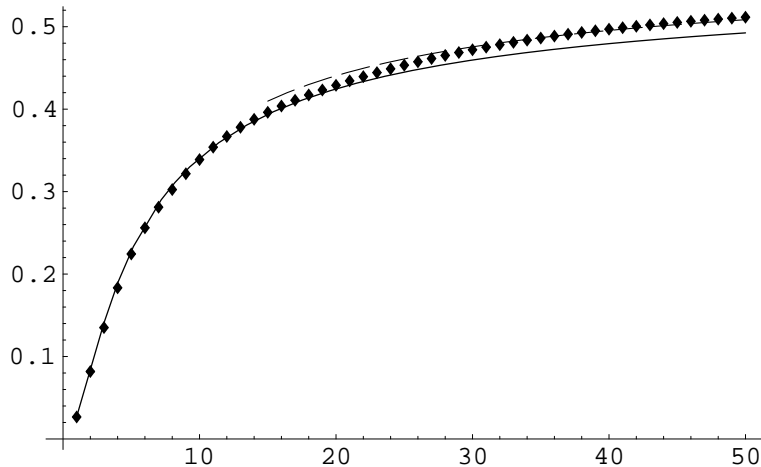
43

Figure 11: Thermodynamic values of the current two-point function at $\xi = 418$ versus $q$. The solid line is the $2+4$ particle form factor result and the dashed line is the absolute upper limit.

might be tempted to regard this as superfluous. However if one were to take these data as representing the continuum limit one would have to conclude that the XY QFT does not coincide with the O(2) bootstrap theory! This is because, in contrast to the $g_{\mathrm{R}}$ measurement, the statistical errors here are very small and the data differ significantly from the bootstrap result. Moreover, as explained below, the truncation error in the bootstrap computation is under good control. The situation is illustrated in Figure 11.

In general it is difficult to strictly control the systematic error in a form factor computation caused by the truncation in the number of intermediate particles. One only knows that the truncated result provides a strict lower bound on the exact answer, since (for a two-point function) all multi-particle contributions are positive. In the O(2) model however we also have a strict upper bound. This is because the exact $I(q)$ is known to be increasing and to approach the value $2/\pi \approx 0.637$ at infinite momentum; c.f. (2.17). On the other hand the 2+4 particle approximation is likewise increasing and approaches 0.621 at infinity; the difference 0.016 is an upper bound on the error made by the truncation, because also the higher particle contributions are monotonically increasing. The true value of the bootstrap function $I(q)$ is somewhere between the 2+4 approximation and this approximation + 0.016, shown as a dashed line in Fig. 11. For the relatively low momentum range we are interested in, the true value is probably closer to the 2+4 value than to the upper limit.

If we use all our data to perform an extrapolation to infinite correlation length, the

situation changes drastically. We assume a cutoff dependence asymptotically linear in $Q$

$$I(q; K, \infty) = I(q) + I'(q)\, Q + O(Q^2)\,, \tag{6.12}$$

and extrapolate our measurements to infinite correlation length by means of a linear fit to the data points corresponding to families 10, 11 and 12. Our thermodynamic data (for families 2,4,6,9,10,11,12) together with this fit is shown in Figures 12 and 13 for $q = 5, 15, 25$. For concreteness we used $u = 1.33$, corresponding to $n_{\text{skip}} = 4$ in Table 6, in all our fits. Varying $u$ around this value we observed that our results are rather insensitive to the precise choice of $u$ in the range 1.2 - 1.5.
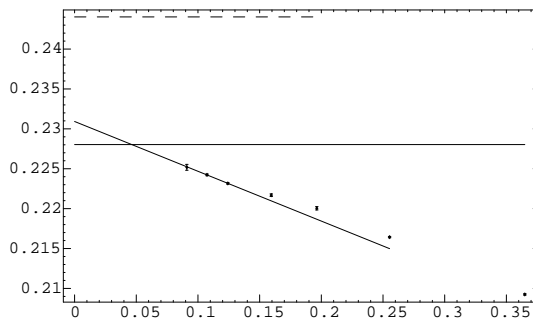


Figure 12: Thermodynamic values of the current correlation function for lattice families 2,4,6,9,10,11,12 for $q = 5$ versus $Q$. The solid horizontal line shows the $2 + 4$ form factor result and the dashed horizontal line is the absolute upper limit. The linear fit is based on the three biggest lattices, corresponding to families 10, 11 and 12.
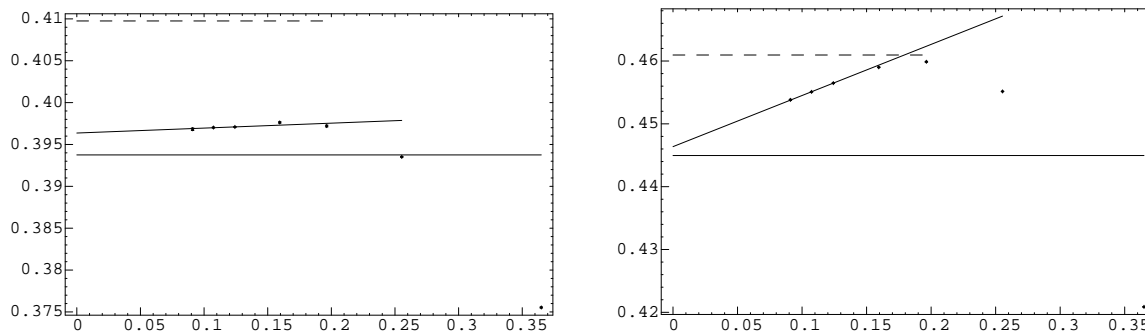


Figure 13: Left: same as Fig. 12 for $q = 15$. Right: same as Fig. 12 for $q = 25$.

From these figures one infers that the approach to the continuum limit, for $q > 10$, is non-monotonic. While this is not unusual in itself, it is most remarkable that for the momentum range $q > 20$, the turning point is around $\xi \sim 40$, a rather large value. Beyond the turning point the data behave as expected and follow a curve that is approximately

linear in $Q$. If we extrapolate our measurements to the continuum limit using the linear fit, the extrapolated points agree reasonably well with the form factor calculation. This is shown in Figure 14, which is one of the main results of this paper. According to this figure the current two point function of the XY QFT is very close to that of the O(2) bootstrap theory. The absolute difference between the extrapolated points and the 2+4 FF result is in the range [0.0003,0.0032]. This difference is positive and much less than 0.016, consistent with the hypothesis that it is due to higher particle contributions.
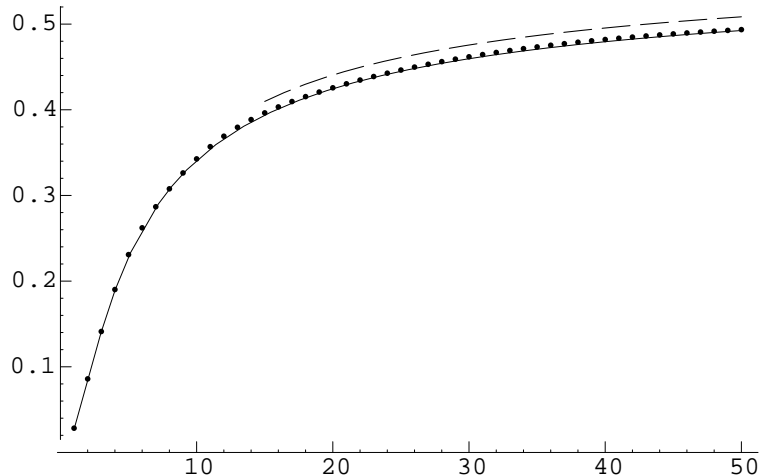


Figure 14: Thermodynamic values of the current two-point function extrapolated to the continuum limit versus $q$. The solid line is the 2+4 particle form factor result and the dashed line is the absolute upper limit.

Not only the extrapolated continuum values $I(q)$ but also the coefficient $I'(q)$ governing the rate of approach can be compared to theory. In the theoretical framework presented in ref.[4] (and recalled in Section 4) this coefficient can be calculated from the continuum SG theory. In [4] this was done in asymptotically free perturbation theory at two-loop order. This is expected to be valid for large momenta subject to the additional constraint [4] $\log q \ll \sqrt{3/2Q}$. Taking $Q \sim 0.1$ our data for $10 < q < 50$ are just in the window of validity. Here we calculated the leading 2-particle contribution to the first correction coefficients using the known [24] 2-particle form factor of the Noether current in the SG theory. In the lattice theory we define $I'(q)$ as the slope of the linear fit on the data for the 3 largest lattice families, 10,11,12. (Recall that all our results correspond to the choice $u = 1.33$.) The comparison with the theoretical results is shown in Figure 15. The agreement is quite remarkable (for the value of $u$ chosen). In particular both analytical computations predict a change of sign in $I'(q)$ between $q = 10$ and $q = 20$, which is indeed

46

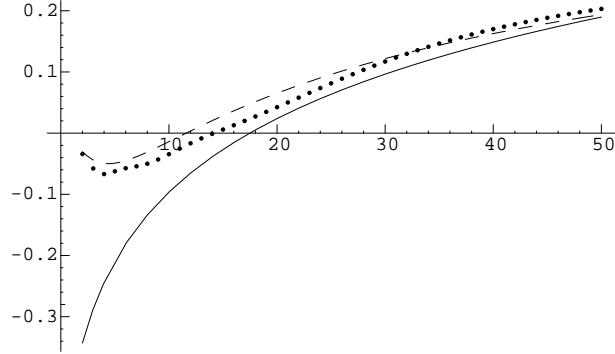observed for the fitted numbers obtained from the MC measurements.



Figure 15: Fitted values of the coefficients $I'(q)$ versus $q$. The solid curve is the perturbative result of [4] and the dashed curve is the leading (2-particle) form factor contribution.

## 6.4 The spin correlation function

Finally we consider the two-point correlation function of the spin operator in Fourier space. While the current correlator had to be subtracted, the spin correlator has to be normalized (multiplicatively) before it can be compared to analytical calculations. We define

$$G^{(\mu)}(q) = \frac{G_0(q)}{G_0(\mu)}, \tag{6.13}$$

where $G_0(q)$ is the bare spin correlator. Traditionally one takes $\mu = 0$, which amounts to normalizing the spin correlator with the susceptibility $\chi$. A problematic feature of this definition is that, just like with the current defined by the SUB method, the statistical errors are big, dominated by the large error of $\chi$. We thus introduced $\hat{G}^{(\mu)}(q) := (q/\mu)^2 G^{(\mu)}(q)$, whose values are closer to unity, and decided to take $\mu = 5$. For $q > 5$ this leads to much smaller errors, in many cases smaller by a factor 3-4. We adopted this unusual choice of normalization because in this paper we focus our attention to the range $q > 5$. The reason for concentrating on this range is that it is here the cutoff effects show interesting non-monotonic behaviour. (For the low momentum range $q < 5$ it would be better to take the normalization at $\mu = 0$, but this is not investigated here.)

Adopting the normalization at $q = 5$ the FS analysis is analogous to the current case. The FS scaling hypothesis is applicable and allows one to extrapolate $\hat{G}^{(5)}(q)$ to thermodynamic lattices. The results are shown in Figures 16, 17 and 18 for $q = 15$, 25 and 35, respectively. Again, similarly to the current case, one sees a non-monotonic approach to

47

the continuum limit, with a turning point which is for $q > 20$ around $\xi \sim 100$. The actual points are still significantly away from the analytical prediction, but beyond the turning point they move into the right direction. We did not attempt to fit a linear function to the data but our results for the spin correlator are not inconsistent with the form factor bootstrap.
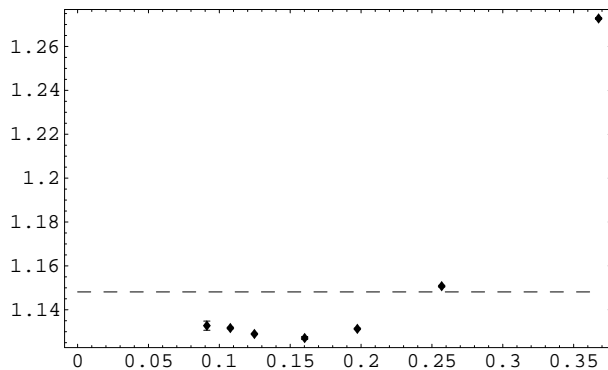


Figure 16: Thermodynamic values of the spin correlation function $\hat{G}^{(5)}(15)$ for lattice families 2, 4, 6, 9, 10, 11 and 12 versus $Q$. The dashed line shows the $1 + 3$ form factor result.
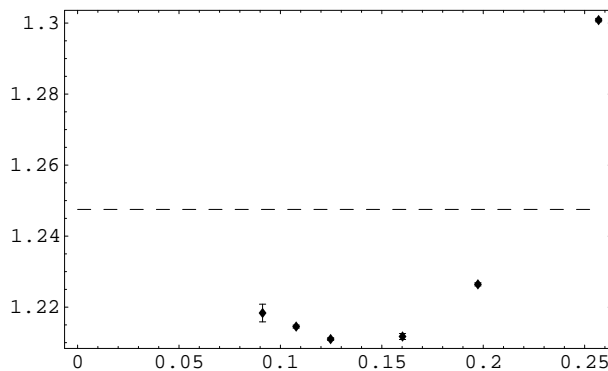


Figure 17: Thermodynamic values of the spin correlation function $\hat{G}^{(5)}(25)$ for lattice families 4, 6, 9, 10, 11 and 12 versus $Q$. The dashed line shows the $1 + 3$ form factor result.
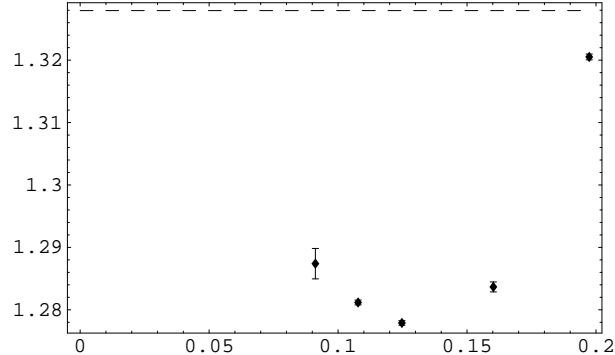
Figure 18: Thermodynamic values of the spin correlation function $\hat{G}^{(5)}(35)$ for lattice families 6, 9, 10, 11 and 12 versus $Q$. The dashed line shows the $1+3$ form factor result.

## 7. Conclusion

Since we already surveyed our motivation and some of the theoretical issues involved in the introduction, let us return here to the question raised in the title. Screening the comparison between bootstrap and lattice theory for the various quantities considered, we would tend to answer the question in the affirmative. Probably the strongest Pro argument stems from the intrinsic coupling $g_R$. The final results in both approaches have an estimated (systematic) error of less than one percent, so that the good agreement is remarkable. For the two-point function of the Noether-current the prediction [4] for the lattice artifacts could be tested. After, and only after, the lattice artifacts are taken into account a good and non-trivial agreement with the form factor result emerges. A final decision whether the remaining small differences are due to the neglected higher particle contributions or signify in fact a true difference of the two constructions cannot be reached at this stage. Quantitatively the least convincing are the phase shift results. However in the lattice framework measurements of the phase shifts are technically difficult and here, as in other models, mainly the qualitative features at low energies can be probed. But the latter do agree with the bootstrap prediction. Each comparison considered separately certainly leaves room for doubt, but collectively they do suggest that the continuum limit of the XY model and the O(2) bootstrap theory are the same QFT.

Concerning future work, a more detailed exploration of the superselection structure should be interesting. The new parafermionic superselection sector found here is probably accompanied by a third ('disorder-like') sector. Their interplay e.g. on the level of the operator product expansion as well as an explicit field theoretical construction remains to be found. Finally, as a test case for other sigma-models, it would be important to understand which

quantities in the XY QFT can be understood, qualitatively or quantitatively, in terms of a perturbed conformal field theory description.

# A. Quantum group covariant form factors

Here we derive the necessary and sufficient conditions (3.13) on the statistics phases that ensure the quantum group covariance of the form factors. The additional conditions like (3.27) required for multiplets transforming irreducibly are also detailed.

To fix our conventions we begin by recalling a few definitions for the action of $\mathcal{U}_q(su(2))$ on some irreducible representation. Background material on quantum groups in 2-dimensional physics can be found in the book [18]. The Hopf algebra $\mathcal{U}_q(su(2))$ is generated by $X_\pm$, $H$ that act for generic $q$ on an irreducible spin $j$ module according to

$$X_\pm |j, m\rangle = \sqrt{[j \mp m]_q [j \pm m + 1]_q}\, |j, m \pm 1\rangle\,,$$
$$H|j, m\rangle = 2m\, |j, m\rangle\,. \tag{A.1}$$

Here $|j, m\rangle$, $m \in \{-j, -j + 1, \ldots, j - 1, j\}$ denotes a basis of the $(2j + 1)$-dimensional irreducible module $\mathbf{2j + 1}$, and $[n]_q = (q^n - q^{-n})/(q - q^{-1})$. For $q = -e^{-i\pi/p}$, $p \geq 3$, an upper bound on the allowed isospins $j$ exists. It reads $j \leq p/2 - 1$ and is related to an enlarged center; see e.g. [2]. To the best of our knowledge the case $q = -1$ has not been studied explicitly in the literature, but it is not hard to work out the aspects needed here. First, as a Lie algebra $\mathcal{U}_{-1}(su(2))$ is isomorphic to $su(2)$, but the co-multiplication differs by signs. Guided by the sample computations presented below and the formal $p \to \infty$ limit of the above relation, we expect that for $q = -1$ no trunction of the allowed isospins occurs. For definiteness we fix the roots $q^{1/2} = i$, $q^{-1/2} = -i$.

For generic $q$ the comultiplication of $\mathcal{U}_q(su(2))$ is

$$\Delta X_\pm = X_\pm \otimes q^{H/2} + q^{-H/2} \otimes X_\pm\,,$$
$$\Delta H = H \otimes \mathbb{1} + \mathbb{1} \otimes H\,, \tag{A.2}$$

for $q \to -1$ we define it with the above choice of roots. For $j = 1/2$ we write $|\pm\rangle = |1/2, \pm 1/2\rangle$ for the basis of the defining representation $\mathbf{2}$. In the $n$-fold tensor product $\mathbf{2}^{\otimes n}$ we write $|\alpha_n, \ldots, \alpha_1\rangle := |\alpha_n\rangle \otimes \ldots \otimes |\alpha_1\rangle$, $\alpha_j \in \{\pm\}$, for the natural basis. The 'charged' components of a form factor are introduced as the coefficients with respect to this basis, i.e.

$$|f\rangle = \sum_{\alpha_n, \ldots, \alpha_1} f_{\alpha_n \ldots \alpha_1} |\alpha_n \ldots \alpha_1\rangle\,. \tag{A.3}$$

By construction the quantum group generator $H^{\otimes n}$ is diagonal on this basis and its eigenvalues $e := \alpha_n + \ldots + \alpha_1$ are the U(1) charges used in section 2. The raising and

lowering operators $\Delta^{(n)}X_\pm$ act as a $2^n \times 2^n$ matrix $\Sigma_\pm$ on the basis $|\alpha_n, \ldots, \alpha_1\rangle$. We choose a lexicographical ordering of the basis vectors that is symmetric under the flip $\alpha_j \to -\alpha_j$. Then $\Sigma_- = \Sigma_+^T$. Further there is an induced action on the coefficients $f_{\alpha_n\ldots\alpha_1}$ in (A.3) which is implemented by $\Sigma_-$ for $\Delta^{(n)}X_+$ and by $\Sigma_+$ for $\Delta^{(n)}X_-$. The $2^n \times 2^n$ matrices $\Sigma_\pm$ are triangular and 'sparse' with only a few blocks different from zero. The block structure arises because evidently $\Delta^{(n)}X_\pm$ maps the charge $e$ sector into the charge $e \pm 2$ sector. Explicitly the matrix $\Sigma_-$ acts on the form factor components as

$$\Sigma_- : \quad f_{\alpha_n\ldots\alpha_1} \quad \longrightarrow \quad e^{i\frac{\pi}{2}(e-1)} \sum_{j=1}^{n} \left(\frac{1+\alpha_j}{2}\right) (-1)^{n-j} f_{\alpha_n\ldots-\alpha_j\ldots\alpha_1} , \tag{A.4}$$

and similarly for $\Sigma_+$. The mapping (3.14) could be used to 'untwist' the $SU_{-1}(2)$ co-multiplication, i.e. to remove the phases in (A.4). We refrain from doing so because the 'untwisting' does not induce a physically interesting correspondence between the form factor sequences of the $SU(2)$ and the $SU_{-1}(2)$ bootstrap theories.

As usual the n-particle form factors carry a representation of the permutation group $S_n$. Its representation matrices are $2^n \times 2^n$ matrices $L_s(\theta)$, $s \in S_n$. The quantum group invariance of the S-matrix (3.7) generalizes to

$$\Sigma_\pm L_s(\theta) = L_s(\theta) \Sigma_\pm , \qquad \forall\, s \in S_n . \tag{A.5}$$

For completeness let us note the explicit definition. One sets

$$L_{s_j}(\theta)_{\alpha_n\ldots\alpha_1}^{\beta_n\ldots\beta_1} = \delta_{\alpha_n}^{\beta_n} \ldots S_{\alpha_{j+1}\alpha_j}^{\beta_j\,\beta_{j+1}}(\theta_{j+1,j}) \ldots \delta_{\alpha_1}^{\beta_1} , \quad j = 1, \ldots n-1 , \tag{A.6}$$

for the generators $s_1, \ldots, s_{n-1}$, acting by $s_j(\theta_n, \ldots, \theta_1) = (\theta_n, \ldots, \theta_j, \theta_{j+1}, \ldots, \theta_1)$ on the rapidities $\theta := (\theta_n, \ldots, \theta_1)$. By means of $L_{ss'}(\theta) = L_s(\theta)L_{s'}(s^{-1}\theta)$ this extends to all $s, s' \in S_n$. The invariance (A.5) clearly entails that the form factor Eq. (3.9a) (and its generalization to generic $s \in S_n$) are covariant under the quantum group action.

It is natural to ask whether the same can be achieved for the cyclic form factor equations (3.9b). In that case the cyclic Eqs in the charge $e$ sector

$$f_{\alpha_n\ldots\alpha_1}(\theta_n + 2\pi i, \theta_{n-1}, \ldots, \theta_1) = \eta_{\alpha_n}(e)\, f_{\alpha_{n-1}\ldots\alpha_1\alpha_n}(\theta_{n-1}, \ldots, \theta_1, \theta_n) , \tag{A.7}$$

with $e = \alpha_n + \ldots + \alpha_1$ and those in the charge $e \pm 2$ sector would again be compatible with the quantum group symmetry. Explicitly this means that starting from (A.7) and

52

performing e.g. the substitutions (A.4) the result should be an identity by virtue of the cyclic Eq. in the charge $e \pm 2$ sectors. This condition gives rise to a set of overdetermined relations among the phases $\eta_\alpha(e)$, – which turn out to be self-consistent. Using (A.4) the solution (3.13) can be verified.

Finally we turn to the residue equations. Consistency requires that the inverse of the matrix $\Gamma_\alpha^\beta$ in (3.9b) appears on the right hand side, irrespective of its concrete form. In the charged basis and for $n \geq 3$ one has:

$$\frac{i}{2}\mathrm{res}_{\theta_n=\theta_{n-1}+i\pi} f_{\alpha_n\ldots\alpha_1}(\theta_n,\ldots,\theta_1) \tag{A.8}$$
$$= \delta_{\alpha_n+\gamma}\left[\eta_\gamma(e)^{-1}L_{s_{n-2}\ldots s_1}(\theta)^{\beta_{n-2}\beta_{n-3}\ldots\,\beta_1\gamma}_{\alpha_{n-1}\alpha_{n-2}\ldots\,\alpha_2\alpha_1} - \delta^\gamma_{\alpha_{n-1}}\delta^{\beta_{n-2}}_{\alpha_{n-2}}\ldots\delta^{\beta_1}_{\alpha_1}\right] f_{\beta_{n-2}\ldots\beta_1}(\theta_n-2,\ldots,\theta_1) \ .$$

Here $e = \alpha_n + \ldots + \alpha_1 = \beta_{n-2} + \ldots + \beta_1$ refers to the charge sector. For the specific choice of phases (3.13) these Eqs can be seen to be likewise quantum group covariant.

In summary there exists a preferred (and up a normalization uniquely determined) choice of the statistics phases $\eta_\alpha(e)$ for which the form factor equations (3.9), (A.9) are covariant with respect to the quantum group $\mathcal{U}_{-1}(su(2))$. This means its solutions can be grouped into multiplets that transform covariantly under the symmetry group, and one can restrict attention to those transforming irreducibly. Technically the irreducibility condition can be encoded into a parameterization of the form factors that is adapted to the embedding of the irreducible spin $j$ module $\mathbf{2j+1}$ into $\mathbf{2}^{\otimes n}$, including multiplicities. Essentially it amounts to determining the generalized Clebsch-Gordon coefficients.

To faciliate the comparison with the familiar $\mathcal{U}_1(su(2)) = su(2)$ case we first consider the decomposition for generic $q$ and specialize to $q = -1$ only at the end. Thus let $\mathbf{2}$ again denote the defining two-dimensional representation of $\mathcal{U}_q(su(2))$ and consider the decomposition of $\mathbf{2}^{\otimes n}$ into irreducible representations. It assumes the familiar form

$$\mathbf{2}^{\otimes n} = \bigoplus_{j_0 \leq j \leq n/2} m_j(n)(\mathbf{2j+1}) \ , \tag{A.9}$$

where $m_j(n)$ is the multiplicity with which $\mathbf{2j+1}$ occurs and $j_0 = 0, 1/2$ for $n$ even,odd, respectively. For generic $q$ these multiplicities are the same as for $su(2)$, only the Clebsch Gordon coefficients differ. As outlined before we expect the limit $q \to -1$ to be regular in the sense that no truncation of the isospins occurs and that the multiplicities $m_j(n)$ are the same as in the undeformed case. The multiplicities then are conveniently computed

from a generalized 'Pascal triangle' described by the recursion relations

$$m_{n/2}(n) = 1 \ , \quad m_j(n) = 0 \ , \quad j < 0 \ ,$$

$$m_j(n) = m_{j-1/2}(n-1) + m_{j+1/2}(n-1) \ , \quad j = j_0, \ldots, n/2 \ . \qquad \text{(A.10)}$$

The highest weight conditions $\Delta^{(n)} X_+ v = 0$, $v \in \mathbf{2}^{\otimes n}$, are readily solved and yield $m_j(n)$ linearly independent solutions on each of which a spin $j$ multiplet can be based.

Below we list for $n = 2, 3, 4$ a basis for the spin $j$ sector in $\mathbf{2}^{\otimes n}$. The multiplicites are taken into account by displaying a $m_j(n)$-dimensional family of highest weight vectors.

$n = 2$:

$j = 0:$ $\quad q^{1/2}|+-\rangle - q^{-1/2}|-+\rangle \ ,$

$j = 1:$ $\quad |++\rangle \ , \quad \Sigma_-|++\rangle \sim q^{1/2}|-+\rangle + q^{-1/2}|+-\rangle \ , \quad \Sigma_-^2|++\rangle \sim |--\rangle \ .$

$n = 3$:

$j = 1/2:$ $\quad v_{1/2} = \lambda_1|-++\rangle + \lambda_2|+-+\rangle + \lambda_3|++-\rangle \ , \quad q^2\lambda_1 + q\lambda_2 + \lambda_3 = 0 \ ,$

$\quad\quad\quad \Sigma_- v_{1/2} = (\lambda_2 + q^{-1}\lambda_1)|+--\rangle + (\lambda_1 + \lambda_3)|-+-\rangle + (q\lambda_1 + \lambda_2)|--+\rangle \ ,$

$j = 3/2:$ $\quad \Sigma_-^k|+++\rangle \ , \quad k = 0, 1, 2, 3 \ .$

$n = 4$:

$j = 0:$ $\quad v_0 = |--++\rangle - (q - q^{-1})|-+-+\rangle - |-++-\rangle - |+--+\rangle + q^2|++--\rangle \ ,$

$\quad\quad\quad v_0' = q^{-1}|-+-+\rangle + |-++-\rangle + |+--+\rangle - q|+-+-\rangle \ ,$

$j = 1:$ $\quad v_1 = \lambda_1|-+++\rangle + \lambda_2|+-++\rangle + \lambda_3|++-+\rangle + \lambda_4|+++-\rangle \ ,$

$\quad\quad\quad q^3\lambda_1 + q^2\lambda_2 + q\lambda_3 + \lambda_4 = 0 \ ,$

$\quad\quad\quad \Sigma_- v_1 \sim q(q\lambda_1 + \lambda_2)|--++\rangle + q(\lambda_1 + \lambda_3)|-+-+\rangle + (\lambda_3 + q\lambda_4)|-++-\rangle$

$\quad\quad\quad\quad + (q\lambda_2 + \lambda_3)|+--+\rangle + (\lambda_2 + \lambda_4)|+-+-\rangle + (\lambda_1 + q^{-1}\lambda_4)|++--\rangle \ .$

$\quad\quad\quad \Sigma_-^2 v_1 = q^2\lambda_1|+---\rangle + q^2[\lambda_2 + (q - q^{-1})\lambda_1]|-+--\rangle$

$\quad\quad\quad\quad + [\lambda_3 - (q - q^{-1})\lambda_4]|--+-\rangle + \lambda_4|---+\rangle \ ,$

$j = 2:$ $\quad \Sigma_-^k|++++\rangle \ , \quad k = 0, 1, 2, 3, 4 \ .$

To illustrate the use of this table let us look at the $n = 3$, $j = 1/2$ entry. The form factor components $f_1, f_2, f_3$ in (3.23) play the role of the $\lambda$'s and for $q = -1$ one obtains (3.27).

54

## B. 3-particle Form Factors

Here we construct the 3-particle form factors of the spin and the parafermion field by an adaptation of the technique of [3]. From the SG viewpoint these fields are nonlocal which is why they have not been considered in [3]. All even particle form factors of the SG fields were constructed by Smirnov [43] where also the Bethe ansatz technique instrumental in [3] is implicit; see also [47] for related results in the mathematical literature.

Adapting theorem 4.1 of [3] the 3-particle FF can be represented as the contour integral

$$f^\alpha_{\epsilon_3\epsilon_2\epsilon_1}(\theta_3, \theta_2, \theta_1) = Y(\theta_3, \theta_2, \theta_1) \int_{\mathcal{C}} du\, \gamma^\alpha_{\alpha_1\alpha_2}(\theta_3, \theta_2, \theta_1; u) v_{\beta_3\beta_2\beta_1}$$
$$S^{\beta_1\gamma_1}_{\epsilon_1\alpha_1}(\theta_1 - u) S^{\beta_2\gamma_2}_{\epsilon_2\gamma_1}(\theta_2 - u) S^{\beta_3\alpha_2}_{\epsilon_3\gamma_2}(\theta_3 - u)\,. \tag{B.1}$$

Here

$$Y(\theta_3, \theta_2, \theta_1) = y(\theta_3 - \theta_2)\, y(\theta_3 - \theta_1)\, y(\theta_2 - \theta_1)\,, \tag{B.2}$$

and the only nonvanishing component of $\gamma^\alpha_{\alpha_1\alpha_2}$ is

$$\gamma^+_{+-}(\theta_3, \theta_2, \theta_1; u) = \mathcal{N} e^{s(\theta_1+\theta_2+\theta_3-2u)} \prod_{m=1}^{3} \frac{\phi(\theta_m - u)}{S_2(\theta_m - u)}\,, \tag{B.3}$$

where

$$\mathcal{N} = \frac{i}{4\pi^{11/2}}\, e^{-\Delta(0)} e^{-i\pi s}\,, \qquad \phi(\theta) := \Gamma\left(\frac{1}{2} + \frac{x}{2\pi i}\right) \Gamma\left(-\frac{x}{2\pi i}\right)\,. \tag{B.4}$$

Finally the "pseudo-vacuum" vector is

$$v_{\beta_3\beta_2\beta_1} = \delta_{\beta_3+}\delta_{\beta_2+}\delta_{\beta_1+}\,. \tag{B.5}$$

The integration contour $\mathcal{C}$ consists of several pieces. First, there are three small clockwise circles around the three points $\theta_1, \theta_2$ and $\theta_3$. In addition $\mathcal{C}$ also contains a line integral parallel to the real axis such that the integration path goes between $\theta_m - i\pi$ and $\theta_m - 2i\pi$ for all the three $\theta_m$.

Since $\mathcal{C}$ is defined relative to the arguments $\theta_m$, when we analytically continue (B.1) it is best to deform the contour parallel to the arguments. This way it is trivial to see that the solution satisfies (3.8). It is also relatively easy to see that the Bethe Ansatz like construction (B.1) ensures that (3.9a) is also satisfied, independently of the contour $\mathcal{C}$. (To show this one has to use the Yang-Baxter equation satisfied by the S-matrix.) It is more difficult to verify (3.9b) because here one has to take into account that the contours

are different on the two sides of the equation. Similarly for the residue equations (3.25) the contour is different from the original $\mathcal{C}$.

Inserting the S-matrix (3.1) Eq. (B.1) can be rewritten as

$$f_m(\theta_3, \theta_2, \theta_1) = \mathcal{N} Y(\theta_3, \theta_2, \theta_1) \int_{\mathcal{C}} du\, e^{s(\theta_1+\theta_2+\theta_3-2u)} \left[ \prod_{k=1}^{3} \phi(\theta_k - u) \right] t_m(\theta_3, \theta_2, \theta_1; u), \quad \text{(B.6)}$$

where

$$
\begin{aligned}
t_1(\theta_3, \theta_2, \theta_1; u) &= \frac{\theta_3 - u}{i\pi - \theta_3 + u} \frac{\theta_2 - u}{i\pi - \theta_2 + u} \frac{i\pi}{i\pi - \theta_1 + u}, \\
t_2(\theta_3, \theta_2, \theta_1; u) &= \frac{\theta_3 - u}{i\pi - \theta_3 + u} \frac{i\pi}{i\pi - \theta_2 + u}, \\
t_3(\theta_3, \theta_2, \theta_1; u) &= \frac{i\pi}{i\pi - \theta_3 + u}.
\end{aligned}
\quad \text{(B.7)}
$$

Next we examine whether the solution (B.7) is compatible with $SU_{-1}(2)$ symmetry, which requires the vanishing of the linear combination (3.27). This can be written as

$$\zeta(\theta_3, \theta_2, \theta_1) = \mathcal{N} Y(\theta_3, \theta_2, \theta_1) \left[ z_1(\theta_3, \theta_2, \theta_1) + z_2(\theta_3, \theta_2, \theta_1) \right], \quad \text{(B.8)}$$

where

$$z_1(\theta_3, \theta_2, \theta_1) = \int_{\mathcal{C}} e^{s(\theta_1+\theta_2+\theta_3-2u)} \left[ \prod_{k=1}^{3} \frac{\theta_k - u}{i\pi - \theta_k + u} \phi(\theta_k - u) \right], \quad \text{(B.9)}$$

$$z_2(\theta_3, \theta_2, \theta_1) = \int_{\mathcal{C}} e^{s(\theta_1+\theta_2+\theta_3-2u)} \left[ \prod_{k=1}^{3} \phi(\theta_k - u) \right]. \quad \text{(B.10)}$$

Using the identity

$$\frac{z}{i\pi - z} \phi(z) = \phi(z - 2\pi i) \quad \text{(B.11)}$$

(B.9) can be rewritten as

$$z_1(\theta_3, \theta_2, \theta_1) = e^{4\pi i s} \int_{\mathcal{C}+} e^{s(\theta_1+\theta_2+\theta_3-2u)} \left[ \prod_{k=1}^{3} \phi(\theta_k - u) \right], \quad \text{(B.12)}$$

where the contour $\mathcal{C}+$ is shifted by $2\pi i$, i.e. it consists of three small circles around $\theta_m + 2\pi i$ and the line integral goes between $\theta_m + i\pi$ and $\theta_m$. From (B.4) we can see that the small circles do not contribute here since the integrand is regular there. The only

relevant singularities are those at $\theta_m$ and it is easy to see that the contribution of the shifted line integral is precisely the same as that of $\mathcal{C}$. We thus have

$$\zeta(\theta_3, \theta_2, \theta_1) = (\eta^2 + 1)\mathcal{N}Y(\theta_3, \theta_2, \theta_1)z_2(\theta_3, \theta_2, \theta_1) \,. \tag{B.13}$$

This proves the assertion after (3.27). Remarkably the quantum group invariance is not visible on the level of the integrand in (B.1) but only after the integral has been performed. In addition this fixes the value of the spin to be $s = \pm 1/4$, without $\mathrm{mod}(1/2)$ ambiguities. This is because the integral in (B.1) exists for $|s| < 3/4$ only.

## C. 4-particle Form Factors of the Noether Current

The form factors of the Noether current can be found in Smirnov's book [43]. We have adapted this result to our notations and conventions for the 4-particle case.

Let us introduce the reduced form factors $g$ that are defined by

$$f_{\epsilon_1\epsilon_2\epsilon_3\epsilon_4}(\theta_1, \theta_2, \theta_3, \theta_4) = Y(\theta_1, \theta_2, \theta_3, \theta_4)g_{\epsilon_1\epsilon_2\epsilon_3\epsilon_4}(\theta_1, \theta_2, \theta_3, \theta_4) \,, \tag{C.1}$$

where

$$Y(\theta_1, \theta_2, \theta_3, \theta_4) = \prod_{i<j} y(\theta_i - \theta_j) \,. \tag{C.2}$$

Using the $O(2)$ symmetry and charge conjugation, we need only the following components:

$$\begin{aligned}
g_{++--}(\theta_1, \theta_2, \theta_3, \theta_4) &= -g_{--++}(\theta_1, \theta_2, \theta_3, \theta_4) \,, \\
g_{+--+}(\theta_1, \theta_2, \theta_3, \theta_4) &= -g_{-++-}(\theta_1, \theta_2, \theta_3, \theta_4) \,, \\
g_{+-+-}(\theta_1, \theta_2, \theta_3, \theta_4) &= -g_{-+-+}(\theta_1, \theta_2, \theta_3, \theta_4) \,.
\end{aligned} \tag{C.3}$$

Further, using the axioms, we can express everything in terms of a single function $A(\theta_1, \theta_2, \theta_3, \theta_4)$ as follows.

$$\begin{aligned}
g_{++--}(\theta_1, \theta_2, \theta_3, \theta_4) &= A(\theta_1, \theta_2, \theta_3, \theta_4) \,, \\
g_{+--+}(\theta_1, \theta_2, \theta_3, \theta_4) &= A(\theta_4 + 2\pi i, \theta_1, \theta_2, \theta_3)
\end{aligned} \tag{C.4}$$

and

$$g_{+-+-}(\theta_1, \theta_2, \theta_3, \theta_4) = \frac{i\pi + \theta_3 - \theta_4}{\theta_4 - \theta_3}\Big[A(\theta_1, \theta_3 + 2\pi i, \theta_4, \theta_2)$$
$$- \frac{i\pi}{i\pi - \theta_4 + \theta_3}\, A(\theta_1, \theta_4 + 2\pi i, \theta_3, \theta_2)\Big]. \tag{C.5}$$

This function is given by

$$A(\beta_1, \beta_2, \beta_3, \beta_4) = \frac{2ie^{-2\Delta(0)}}{\pi^4}\frac{e^{-\frac{1}{2}\left(\sum_{j=1}^{4}\beta_j\right)}}{\left(\sum_{j=1}^{4}e^{-\beta_j}\right)}p(\beta_1, \beta_2, \beta_3, \beta_4)I(\beta_1, \beta_2, \beta_3, \beta_4)\,, \tag{C.6}$$

where

$$p(\beta_1, \beta_2, \beta_3, \beta_4) = (\beta_1 + \beta_2 - \beta_3 - \beta_4 - 2\pi i)\Big[\prod_{i=1}^{2}\prod_{j=3}^{4}\frac{1}{\beta_i - \beta_j - i\pi}\Big] \tag{C.7}$$

and

$$I(\beta_1, \beta_2, \beta_3, \beta_4) = \int_{-\infty}^{\infty}d\alpha e^{\alpha}\big\{q(\alpha, \beta_1)q(\alpha, \beta_2)x(\alpha, \beta_3)x(\alpha, \beta_4)$$
$$+ x(\alpha, \beta_1)x(\alpha, \beta_2)q(\alpha, \beta_3 + 2\pi i)q(\alpha, \beta_4 + 2\pi i)\big\}\,. \tag{C.8}$$

Here we defined

$$x(\alpha, \beta) = \Gamma\Big(\frac{1}{4} - \frac{\alpha - \beta}{2\pi i}\Big)\Gamma\Big(\frac{1}{4} + \frac{\alpha - \beta}{2\pi i}\Big) = \phi\Big(\beta - \alpha - \frac{i\pi}{2}\Big),$$
$$q(\alpha, \beta) = \Gamma\Big(\frac{1}{4} - \frac{\alpha - \beta}{2\pi i}\Big)\Gamma\Big(\frac{5}{4} + \frac{\alpha - \beta}{2\pi i}\Big)\,. \tag{C.9}$$

# D. Calculation of the subleading correction to $g_{\mathrm{R}}$

The leading contribution to the intrinsic coupling $g_{\mathrm{R}}$ in the O(2) model was calculated in [7]. Here we present the calculation of the most important subleading term reducing the theoretical uncertainty in this quantity to a few per mille. This appendix relies heavily on [7], especially Sections 3, 6 and Appendix C. We use the notations and conventions of that paper.

The first few contributions to $\gamma_4$ for the Ising model and for the O(3) model were also calculated in [7]. Let us compare the results.

| contribution | Ising model | O(3) model |
|:---:|:---:|:---:|
| 121 | $-4.99343$ | $-4.16835$ |
| 123/1 | $-0.01348$ | $-0.01351$ |
| 123/2 | $0.10610$ | $0.11901$ |
| 123/3 | $0.00000$ | $-0.00200$ |
| 141 | $-0.00265$ | $-0.00407$ |

Table 10: The first few contributions to $\gamma_4$. 123/i stand for the contribution of the integrals $V^{(i)}$ for i=1, 2 and 3.

The pattern is strikingly similar for the two models. For the XY model we so far only have the 121 contribution, which is somewhere inbetween the corresponding values for the Ising and the O(3) model. If we assume that the corrections follow the same pattern also for the O(2) model, already the calculation of the 123/2 term yields $\gamma_4$ with a precision better than one percent. We will see that we have all the ingredients necessary for this calculation.

Using the FF axioms and some of the expressions in Appendix C of [7] we have

$$
\begin{aligned}
g^{(3)}(\beta, \alpha_1, \alpha_2) \;=\; & \mathcal{G}^1_{1bb}(i\pi, \beta, -\beta)\, \mathcal{G}^1_{bx_1x_2}(i\pi - \beta, \alpha_1, \alpha_2)\, \mathcal{G}^{*1}_{bx_1x_2}(\beta, \alpha_1, \alpha_2) \qquad \text{(D.1)} \\
& - \; \mathcal{G}^1_{1bb}(i\pi, -\beta, \beta)\, \mathcal{G}^1_{bx_1x_2}(i\pi - \beta, \alpha_1, \alpha_2)\, \mathcal{G}^{*1}_{x_1x_2b}(\alpha_1, \alpha_2, \beta)\,.
\end{aligned}
$$

Now it is easy to see that $g^{(3)}(0, \alpha, -\alpha) = 0$ so

$$
V^{(4)} = 0 \qquad\qquad\qquad \text{(D.2)}
$$

in general. Further using $(D.1)$ in $(C.43)$ of $[7]$ we get

$$g^{(5)}(\beta) \;=\; \mathcal{G}^1_{1bb}(i\pi, \beta, -\beta) \left\{ \mathcal{G}^{*1}_{bb1}(\beta, -\beta, 0) + \mathcal{G}^{*1}_{b1b}(\beta, 0, -\beta) \right\}$$

$$- \;\; \mathcal{G}^1_{1bb}(i\pi, -\beta, \beta) \left\{ \mathcal{G}^{*1}_{b1b}(-\beta, 0, \beta) + \mathcal{G}^{*1}_{1bb}(0, -\beta, \beta) \right\}. \tag{D.3}$$

We see that

$$g^{(5)}(\beta) + g^{(5)}(-\beta) = 0 \,, \tag{D.4}$$

so also for generic $n$

$$V^{(5)} = 0 \,. \tag{D.5}$$

$(D.2)$ and $(D.5)$ together imply that the conjecture $(C.57)$ of $[7]$ is true.

Similarly simplifying $(C.37)$ of $[7]$ gives

$$g^{(2)}(\beta) = \mathcal{G}^1_{1bb}(i\pi, \beta, -\beta)\, \mathcal{G}^{*1}_{bb1}(\beta, -\beta, 0) \tag{D.6}$$

and using this in $(C.36)$ of $[7]$ we have

$$\mathcal{F}^1_{1bb}(i\pi, v, -v)\, \mathcal{F}^1_{bb1}(-v, v, 0)\,. \tag{D.7}$$

It is easy to see that we already have everything that is necessary to compute $(D.7)$ since

$$\mathcal{F}^1_{xy1}(-v, v, 0) = S_{y1;qp}(v)\, f^1_{pqx}(i\pi + v)\,. \tag{D.8}$$

Putting everything together we have

$$V^{(2)} = \frac{1}{64\pi} \int_0^\infty dv\, \frac{\sinh^2 v}{\cosh^4 v}\, e^{H(v)}\, \mathcal{M}(v)\,, \tag{D.9}$$

where

$$H(v) = \Delta(i\pi + v) + \Delta(i\pi - v) + \Delta(2v) + \Delta(-2v) + \Delta(v) + \Delta(-v) - 2\Delta(0) \quad \text{(D.10)}$$

and

$$\begin{aligned}
\mathcal{M}(v) \;=\; & \frac{1}{(i\pi - v)\big[(n-2)v - 2\pi i\big]} \Big\{ K(v)K(i\pi + v)\left[2\pi^2 + n(n-2)v(i\pi - v)\right] \\
& + \;\; 2K(v)L(i\pi + v)\left[(n+1)\pi^2 + (n-2)v(i\pi - v)\right] \\
& + \;\; 2L(v)K(i\pi + v)\left[2\pi^2 + (n-2)v(i\pi - v)\right] \\
& + \;\; 4L(v)L(i\pi + v)\left[2\pi^2 - i\pi v + (2-n)v^2\right] \Big\}.
\end{aligned} \tag{D.11}$$

60

To summarize, using the results of [7] (D.9) in the $n = 2$ case can be represented as

$$V^{(2)} = \frac{1}{3600\pi^7} \int_0^\infty d\theta \frac{\sinh^3 \theta}{\cosh^4 \theta} \left\{ e^{H+D_3+D_1} \sqrt{(4\theta^2 + 25\pi^2)(4\theta^2 + 49\pi^2)} \left[ \frac{A_1}{\theta} + \frac{\pi A_2}{2(\theta^2 + \pi^2)} \right] \right.$$
$$\left. + e^{H+D_5+D_1} (4\theta^2 + 9\pi^2) \left[ \frac{A_1}{\theta} + \frac{3\pi A_2}{2(\theta^2 + \pi^2)} \right] \right\}, \qquad (D.12)$$

where

$$H(\theta) = 2 \int_0^\infty \frac{d\omega}{\omega} \frac{\cos \omega\theta + \cosh \pi\omega (\cos 2\omega\theta + \cos \omega\theta - 1) - 2}{\sinh \pi\omega (1 + e^{\pi\omega})}, \qquad (D.13a)$$

$$D_1(\theta) = \int_0^\infty \frac{d\omega}{\omega} \frac{\cos \frac{\omega\theta}{2} - 1}{2 \sinh \frac{\pi\omega}{2}} k(\omega), \qquad (D.13b)$$

$$D_3(\theta) = \int_0^\infty \frac{d\omega}{\omega} \frac{\cosh \pi\omega \cos \frac{\omega\theta}{2} - \cosh \frac{\pi\omega}{2}}{\sinh \pi\omega} k(\omega), \qquad (D.13c)$$

$$D_5(\theta) = \int_0^\infty \frac{d\omega}{\omega} \frac{\cos \frac{\omega\theta}{2} - \cosh \frac{\pi\omega}{2}}{\sinh \pi\omega} k(\omega). \qquad (D.13d)$$

Further

$$k(\omega) = -e^{-\frac{5}{4}\pi\omega} - e^{-\frac{7}{4}\pi\omega}, \qquad (D.14)$$

and finally

$$A_1 + iA_2 = i(i\pi - 2\theta)(3i\pi + 2\theta)(5i\pi + 2\theta)e^{iD_2(\theta)}, \qquad (D.15)$$

where

$$D_2(\theta) = -\int_0^\infty \frac{d\omega}{\omega} \frac{\sin \frac{\omega\theta}{2}}{2 \cosh \frac{\pi\omega}{2}} k(\omega). \qquad (D.16)$$

Numerically we find

$$V^{(2)} = 0.00724518. \qquad (D.17)$$

Now we are in a position to be able to fill in some O(2) entries in the previous table.

As expected, the available O(2) data follow the same pattern as before. Furthermore the O(2) numbers are in between the O(1) and O(3) ones. So (with some confidence) we can predict the uncalculated (∗) contributions to be close to the avarage of the corresponding Ising and O(3) entries. In this way we get

$$(*) = -0.01786 \pm 0.00893, \qquad (D.18)$$

| contribution | Ising model | O(2) model | O(3) model |
|:---:|:---:|:---:|:---:|
| 121 | $-4.99343$ | $-4.65718$ | $-4.16835$ |
| 123/1 | $-0.01348$ | $*$ | $-0.01351$ |
| 123/2 | $0.10610$ | $0.11592$ | $0.11901$ |
| 123/3 | $0.00000$ | $*$ | $-0.00200$ |
| 141 | $-0.00265$ | $*$ | $-0.00407$ |

Table 11: The first few contributions to $\gamma_4$. 123/i stand for the contribution of the integrals $V^{(i)}$ for i=1, 2 and 3.

where (generously) we allowed for 50% error here. This gives a total $k + l + m = 6$ contribution of

$$0.09806 \pm 0.00893 \,. \tag{D.19}$$

Estimating the $k + l + m \geq 8$ contributions, as usual, to be less than 10% of (D.19) our final estimate is

$$\gamma_4 = -4.559 \pm 0.019 \,. \tag{D.20}$$

We also need the product $\gamma_2 \delta_2$. We have computed numerically the 3-particle contribution to both $\gamma_2$ and $\delta_2$ using the 3-particle form factors constructed in Appendix B. We found

$$\gamma_{2;3} = 0.001813(1) \qquad \text{and} \qquad \delta_{2;3} = 0.00003016(2) \,. \tag{D.21}$$

Thus $\gamma_2 \delta_2 = 1.00184$ and finally we get $g_{\mathrm{R}}$ with an error of a few permille:

$$g_{\mathrm{R}} = 9.10(4) \,. \tag{D.22}$$

## E. Test of random number generators

Since we are interested in achieving numerical precision for many quantities to an accuracy of $< 1\%$, a considerable source of concern to us was the random number generator (RNG). Indeed at an initial stage of this project we found large standard deviations between results obtained by various generators.

Our first test concerned comparison of computations using various RNG's, with exact results on small lattices. The (practically) exact result on a $3 \times 3$ lattice is obtained by discretizing the spins, taking $O(2) \to Z(N)$ and summing over all $N^{V-1}$ terms* in the partition function. The convergence to the $O(2)$ case is extremely (exponentially) fast. As illustration in Table 12 we give the values of the susceptibility for $K = 0.25$, $L = 3$ and $N = 6, \ldots, 10$. Some generators already failed this test. The exact numbers were also useful to check our programs.

| $N$ | $\chi$ |
|----|--------------|
| 6 | 1.7619848372 |
| 7 | 1.7619804581 |
| 8 | 1.7619803546 |
| 9 | 1.7619803525 |
| 10 | 1.7619803524 |

Table 12: The susceptibility of the $Z(N)$ model on a $3 \times 3$ lattice at $K = 0.25$.

As a next step we compared results obtained by different RNG's on larger lattices, see e.g. Table 13 where we tabulated our results for the susceptibility at $K = 1.0$, $L = 256$. Here `rand` is the RNG listed in *Language Reference* XL Fortran for AIX (Version 3 Release 2) and `SGI` is the RNG provided by Silicon Graphics for the SGI 2000 machine. The `nag` (the `g05caf` RNG by Numerical Algorithms Group) and `ranlux` [34] are portable RNG's. The latter has a single- and a double precision version, both with an extra choice, a "luxury parameter". The notations "rlxs_0", "rlxd_1" and "rlxd_2" refer to the precision and the value of the luxury level parameter.

To our knowledge `ranlux` is the only generator known with proven randomness qualities. Unfortunately, for "historical reasons" we used it only in the later stages of the project, while most of other runs were using `nag`. Reassuringly we found in all our tests, that the

---

*Due to the global symmetry one spin can be fixed.

| program | RNG | $\chi$ |
|---------|-----|--------|
| 1 | rand | 1609.5(9) |
| 1 | SGI | 1607.3(9) |
| 1 | nag | 1604.7(8) |
| 2 | nag | 1605.5(9) |
| 2 | rlxd_2 | 1604.1(9) |

Table 13: The susceptibility at $K = 1.0$ and $L = 256$ using different RNG's and two different programs

nag generator produced results consistent with ranlux. The combined nag result (same RNG but different programs) in Table 13 is 1605.1(6), which is only 1-sigma away from rlxd_2. Note however, the rand result is 4.2-sigma away from rlxd_2 while the SGI result is 2.5-sigma away.

Although the latter deviation is still not too serious, the SGI RNG gave also suspicious results on lattices with very large physical size, $z \approx 14$: the data obtained by this RNG were several sigma too high above the FS scaling lines. Since the $z > 10$ data were not needed in the extrapolations anyhow, we simply omitted these data points from Table 4 and did not use them in our fits. Nevertheless, to make sure that the discrepancy was indeed due to the failure of the RNG we remeasured a few of these points with ranlux. Table 14 shows the results for these two RNG's, together with the fits of Table 5. Note that the SGI results show large deviations from both ranlux and the FS fit, especially for the susceptibility, which is always too high, by 5.6 to 7.6 standard deviations.

The only SGI data present in Table 4 are the 4 points at $K = 1.04$ and 1.05 for $z = 4$ and 5. These data, in contrast to the $z = 14$ points, agree with the FS fits. We have also rechecked the $K = 1.04$, $L = 578$ point with rlxs_0 and got $\xi = 142.10(9)$, $\chi = 14142(12)$, $g_{\mathrm{R}} = 7.604(9)$, in good agreement with the SGI results[†] in Table 4 therefore we did not repeat all these measurements with ranlux.

In one of the programs we measured the quantities with the standard estimator along with the improved one, and checked that they agree within the errors. The other program used a Ward identity for checking. Note, however, that the agreement in these quantities does not guarantee yet the correctness of the results: the error of the standard estimator is

---

[†]Note, however, that at these very large correlation length our relative errors are much larger than those at smaller $\xi$.

| $K$ | $L$ | $\xi$ | $\chi$ | $g_{\mathrm{R}}$ | RNG |
|---|---|---|---|---|---|
| 0.92 | 150 | 10.559(3) | 163.110(36) | 8.879(25) | `rand` |
| | | 10.5508(9) | 162.843(13) | 8.864(8) | `nag` |
| | | 10.5499(7) | 162.829(10) | 8.869(6) | `rlxs_0` |
| | | 10.5507(9) | 162.835(12) | 8.871(8) | `rlxd_1` |
| | | 10.5510(11) | 162.840(16) | 8.881(10) | `rlxd_2` |
| | | 10.549(1) | 162.86(26) | 8.877(6) | FS fit |
| 0.97 | 300 | 21.659(6) | 557.41(15) | 8.958(25) | `SGI` |
| | | 21.627(4) | 556.32(11) | 8.952(6) | FS fit |
| 1.0 | 560 | 40.168(13) | 1615.68(48) | 9.037(29) | `SGI` |
| | | 40.107(12) | 1611.78(43) | 9.010(28) | `rlxd_2` |
| | | 40.096(5) | 1611.4(3) | 8.989(6) | FS fits |
| 1.02 | 1000 | 69.647(23) | 4184.5(1.2) | 9.066(34) | `SGI` |
| | | 69.533(24) | 4174.5(1.3) | 8.962(33) | `rlxd_2` |
| | | 69.505(20) | 4173.0(1.4) | 9.026(8) | FS fits |

Table 14: The correlation length and susceptibility for $z \approx 14$ for different RNG's and the corresponding value obtained by finite size (FS) extrapolation taken from Table 5.

usually much larger than that of the improved estimator, while even the bad $z = 14$ results passed the WI test.

# F. Vohwinkel's results for the 2-particle energies

We here reproduce the original data table of Vohwinkel, giving the 2-particle energies obtained nearly 10 years ago [49]. We do not know the reason why Vohwinkel did not publish his results, but it could be that he just confused the assignment of quantum numbers, and so could not match his results with the proposed S-matrix. With the correct identification his data are listed in Table 15.

As mentioned in Section 5 his values for the single particle masses on the lattices with $z >\sim 10$ are in good agreement with ours. It is only on the lattice with $K = 0.97$ and $L = 128$ that our values differ by $\sim 4$ standard deviations.

| $K$ | 0.97 | 0.97 | 0.92 | 0.86 |
|-----|------|------|------|------|
| $L$ | 128 | 256 | 128 | 64 |
| $m$ | 0.04633(2) | 0.04620(1) | 0.09465(3) | 0.1711(1) |
| 2 | 0.1019(2) | 0.0956(2) | 0.1949(3) | 0.353(1) |
| | 0.1612(3) | 0.1149(3) | 0.2334(4) | 0.435(2) |
| | | 0.1481(6) | 0.2982(7) | 0.566(3) |
| | | 0.1872(8) | 0.3760(10) | |
| 1 | 0.1298(1) | 0.1038(4) | 0.2116(4) | 0.389(1) |
| | | 0.1324(4) | 0.2676(7) | 0.510(2) |
| | | 0.1705(6) | 0.3440(20) | |
| 0 | 0.1081(15) | 0.0967(3) | 0.1966(10) | |
| | | 0.1220(8) | 0.2431(20) | |
| | | 0.1614(14) | 0.3143(40) | |

Table 15: Masses and energies obtained by Claus Vohwinkel in 1992

# References

[1] D. J. Amit, Y. Y. Goldschmidt and G. Grinstein, J. Phys. **A13** (1980) 585.

[2] D. Arnaudon, Commun. Math. Phys. **159** (1994) 175.

[3] H. Babujian, A. Fring, M. Karowski and A. Zapletal, Nucl. Phys. B538 (1999) 535.

[4] J. Balog, J. Phys **A34** (2001) 5237.

[5] J. Balog and Á. Hegedűs, J. Phys. **A33** (2000) 6543.

[6] J. Balog, M. Niedermaier, F. Niedermayer, A. Patrascioiu, E. Seiler and P. Weisz, Phys. Rev. **D60** (1999) 094508.

[7] J. Balog, M. Niedermaier, F. Niedermayer, A. Patrascioiu, E. Seiler and P. Weisz, Nucl. Phys. **B583** (2000) 614.

[8] T. Banks, D. Horn, and H. Neuberger, Nucl. Phys. **B108** (1976) 119.

[9] B. Berg and P. Weisz, Nucl. Phys. **B146** (1979) 205;
E. Abdalla, B. Berg and P. Weisz, Nucl. Phys. **B157** (1979) 387.

[10] P. Butera and M. Comi, Phys. Rev. **B54** (1996) 15828.

[11] P. Butera and M. Comi, Phys. Rev. **B47**(1993)11969.

[12] M. Campostrini, A. Pelissetto, P. Rossi and E. Vicari, Nucl. Phys. **B459** (1996) 207;
Nucl. Phys. Proc. Suppl. **47** (1996) 751.

[13] S. Coleman, Phys. Rev. **D11** (1975) 2088.

[14] C. Destri, Phys. Lett. **210B** (1988) 173; Erratum–*ibid* **213B** (1988) 565.

[15] M. Falcioni, G. Martinelli, M. L. Paciello, G. Parisi and B. Taglienti, Nucl. Phys. **B225** (1983) 313.

[16] G. Felder and A. LeClair, Int. J. Mod. Phys. **A7** (1992) 239.

[17] J. Fröhlich and T. H. Spencer, Comm. Math. Phys. **81** (1981) 527.

[18] C. Gomez, G. Sierra, M. Ruiz-Altaba, *Quantum groups in two-dimensional physics*, Cambridge University Press, 1996.

[19] R. Gupta, J. De Lapp, G. G. Batrouni, G. C. Fox, C. F. Baillie and J. Apostolakis, Phys. Rev. Lett. **91** (1988) 1996;
R. Gupta and C. F. Baillie, Nucl. Phys. B (Proc. Suppl.) **20** (1991) 669;
R. Gupta and C. F. Baillie, Phys. Rev. **B45** (1992) 2883;
U. Wolff, Nucl. Phys.**B322** (1989) 759;
R. G. Edwards, J. Goodman, A. D. Sokal, Nucl. Phys. **B354** (1991) 289;
W. Janke and K. Nather, Phys. Lett. **157A** (1991) 11.

[20] P. Hasenfratz, M. Maggiore and F. Niedermayer, Phys. Lett. **B245** (1990) 522;
P. Hasenfratz and F. Niedermayer, Phys. Lett. **B245** (1990) 529.

[21] M. Hasenbusch, M. Marcu and K. Pinn, Physica **A208** (1994) 124.
M. Hasenbusch and K. Pinn, J. Phys. **A30** (1997) 63.

[22] W. Janke, Phys. Rev. **B55** (1997) 3580.

[23] J. V. José, L. Kadanoff, S. Kirkpatrick, and D. Nelson, Phys. Rev. **B16** (1977) 1217.

[24] M. Karowski and P. Weisz, Nucl. Phys. **B139** (1978) 455.

[25] R. Kenna and A. C. Irving, Nucl. Phys. **B485** (1997) 583; Phys. Lett. **B351** (1995) 273.

[26] T. Klassen and E. Melzer, Int. J. Mod. Phys. **A8** (1993) 4131.

[27] R. M. Konik and A. LeClair, Nucl. Phys. **B479** (1996) 619.

[28] J.M. Kosterlitz and D.J. Thouless, J. Phys. **C6** (1973) 1181;
J.M. Kosterlitz, J. Phys. **C7** (1974) 1046.

[29] M. Lashkevich, *Sectors of mutually local fields in integrable models of QFT*, [hep-th/9406118].

[30] A. LeClair and F. Smirnov, Int. J. Mod. Phys. **A7** (1992) 2997.

[31] M. Lüscher und U. Wolff, Nucl. Phys. **B339** (1990) 222.

[32] M. Lüscher, Commun. Math. Phys. **104** (1986) 177.
M. Lüscher, *On a relation between finite size effects and elastic scattering processes*, in: Cargese Summer Inst. 1983, Plenum Press, New York, 1984.

[33] M. Lüscher, Nucl. Phys. **B135** (1978) 1.

[34] M. Lüscher, Comp. Phys. Commun. **79** (1994) 100.

[35] C. Michael, Nucl. Phys. **B259** (1985) 58.

[36] M. Niedermaier, Commun. Math. Phys. **196** (1998) 411.

[37] F. Niedermayer, Ph. Rüfenacht and U. Wenger, Nucl. Phys. **B597** (2001) 413.

[38] A. Patrascioiu and E. Seiler, *Absence of Asymptotic Freedom in nonabelian models* [hep-th/0002153]; *Percolation and the existence of a soft phase in the classical Heisenberg model*, [hep-th/0011199].

[39] A. Patrascioiu and E. Seiler, Phys. Lett. **B417** (1998) 123; Phys. Rev. **E57** (1998) 111.

[40] A. Pelissetto and E. Vicari, Nucl. Phys. **B519** (1998) 626; Nucl. Phys. **575** (2000) 579.

[41] A. Polyakov, Phys. Lett. **B72** (1977) 224.

[42] N. Reshetikhin and F. Smirnov, Commun. Math. Phys. **131** (1990) 157.

[43] F. Smirnov, *Form factors in completely integrable models of quantum field theory*, World Scientific, 1992.

[44] F. Smirnov, Commun. Math. Phys. **132** (1990) 415.

[45] K. Symanzik, Nucl. Phys. **B226** (1983) 187.

[46] H. Swendsen and J. Wang, Phys. Rev. Lett. **58** (1987) 86.

[47] V. Tarasov and A. Varchenko, Amer. Math. Transl. **174** (1996) 235.

[48] J. Villain, J. Physique **36** (1975) 581.

[49] C. Vohwinkel, private communication (1992).

[50] U. Wolff, Phys. Rev. Lett. **62** (1989) 361.

[51] C.H. Woo, Phys. Rev. **D20** (1979) 1880.

[52] A.B. and Al.B. Zamolodchikov, Ann. Phys. **120** (1979) 253; Nucl. Phys. **B133** (1978) 525.

[53] Al. B. Zamolodchikov, Int. J. of Mod. Phys. **A10** (1995) 1125.

[54] J. Zinn-Justin, *Quantum Field Theory and Critical Phenomena*, Oxford, 1989.